A Spectroscopic Survey of Electronic Transitions of C_6H, $^{13}C_6H$, and C_6D

X. Bacalla[a,b], E.J. Salumbides[a,c], H. Linnartz[b], W. Ubachs[a], D. Zhao[a,b,1,*]

[a] *Department of Physics and Astronomy, LaserLaB, VU University Amsterdam, De Boelelaan 1081, NL-1081 HV Amsterdam, The Netherlands*
[b] *Sackler Laboratory for Astrophysics, Leiden Observatory, Leiden University, PO Box 9513, NL-2300 RA Leiden, The Netherlands*
[c] *Department of Physics, University of San Carlos, Nasipit, Talamban, Cebu City 6000, Philippines*

arXiv:1608.00880v1 [physics.chem-ph] 2 Aug 2016

Abstract

Electronic spectra of C_6H are measured in the $18\,950 - 21\,100$ cm^{-1} domain using cavity ring-down spectroscopy of a supersonically expanding hydrocarbon plasma. In total, 19 (sub)bands of C_6H are presented, all probing the vibrational manifold of the $B^2\Pi$ electronically excited state. The assignments are guided by electronic spectra available from matrix isolation work, isotopic substitution experiments (yielding also spectra for $^{13}C_6H$ and C_6D), predictions from *ab initio* calculations as well as rotational fitting and vibrational contour simulations using the available ground state parameters as obtained from microwave experiments. Besides the 0_0^0 origin band, three non-degenerate stretching vibrations along the linear backbone of the C_6H molecule are assigned: the ν_6 mode associated with the C–C bond vibration and the ν_4 and ν_3 modes associated with C≡C triple bonds. For the two lowest ν_{11} and ν_{10} bending modes, a Renner-Teller analysis is performed identifying the $\mu^2\Sigma(\nu_{11})$ and both $\mu^2\Sigma(\nu_{10})$ and $\kappa^2\Sigma(\nu_{10})$ components. In addition, two higher lying bending modes are observed, which are tentatively assigned as $\mu^2\Sigma(\nu_9)$ and $\mu^2\Sigma(\nu_8)$ levels. In the excitation region below the first non-degenerate vibration (ν_6), some $^2\Pi - {}^2\Pi$ transitions are observed that are assigned as even combination modes of low-lying bending vibrations. The same holds for a $^2\Pi - {}^2\Pi$ transition found above the ν_6 level. From these spectroscopic data and the vibronic analysis a comprehensive energy level diagram for the $B^2\Pi$ state of C_6H is derived and presented.

Keywords: hexatriynyl radical, cavity ring-down spectroscopy, isotopic substitution, supersonic plasma discharge

Introduction

The hexatriynyl radical, C_6H, belongs to the best studied linear carbon chain radicals. As several other members in the acetylenic $C_{2n}H$ series, it has been identified in different environments in the interstellar medium.[1–4] Microwave spectroscopic work[5] has provided accurate spectroscopic constants for the $X^2\Pi$ electronic ground state that later were extended to deuterated hexatriynyl[6] (C_6D) as well as to vibrationally excited C_6H.[7] *Ab initio* calculations,[8–10] together with infrared (IR) work,[11] have also been conducted to predict and identify the fundamental vibrational frequencies of C_6H. Recently, the astronomical detection of vibrationally excited C_6H[7,12] and the chemically related C_6H^- anion[13] triggered a renewed spectroscopic interest in this molecule.

The first electronic spectra of C_6H were recorded using matrix isolation spectroscopy;[14,15] results of which guided two gas phase studies.[6,16] An unresolved electronic origin band as well as several hot bands were recorded for a rather high temperature ($T_{\rm rot} \sim 150$ K) using a liquid-nitrogen cooled hollow cathode discharge.[16] After this, a study of a supersonically expanding and adiabatically cooled plasma resulted in a full rotational analysis of the two spin-orbit components of the $^2\Pi$–$X^2\Pi$ origin band spectrum for both C_6H and C_6D radicals.[6] An extended study, presenting more accurate data for the electronic origin band as well as a Renner-Teller analysis for the $\{11\}_1^1$ $\mu^2\Sigma - \mu^2\Sigma$ vibronic hot band, was presented several years later.[17] In the optical spectra only the $^2\Sigma$ vibronic component of the ν_{11} mode was observed, in contrast to the $^2\Delta$ component, which was detected in the microwave spectrum,[7] but which is most likely too energetic (~ 100 cm^{-1}) to be observed in cold jet expansions. The same holds for the low-lying electronic state with $^2\Sigma$ symmetry, at an excitation energy of $\sim 1\,774$ cm^{-1}, which was observed in a photo-detachment study.[18] These states were predicted in *ab initio* electronic structure calculations.[10,19] Harmonic vibrational frequencies of the various modes in C_6H were *ab initio* calculated, yielding the lowest mode, ν_{11}, at some 100 cm^{-1} and the highest mode at about $3\,300$ cm^{-1}.[9] Also of interest is the spectroscopic investigation of the C_6H^+ cation, both in a neon matrix[20] and

* Corresponding author.
Email address: dzhao@ustc.edu.cn (D. Zhao)

[1] Present address: Hefei National Laboratory for Physical Sciences at the Microscale, Department of Chemical Physics, University of Science and Technology of China, 96 Jinzhai Road, Hefei, Anhui 230026, P. R. China.

in the gas phase.[21]

In the present work, cavity ring-down spectroscopy of a supersonically expanding hydrocarbon plasma has been employed in a wider-ranging spectroscopic survey. All spectroscopic features observed are associated with the $B^2\Pi$ electronically excited state and its vibrational modes. From the C_6H origin band at $18\,980$ cm^{-1} towards higher wavenumbers, several new spectral features have been observed and found to originate from C_6H as well. Also, a substantial number of $^{13}C_6H$ (full ^{13}C substitution) and C_6D bands has been observed for the first time.

Experiment

The experimental setup and the measurement procedure are similar to those described before.[17,22] The carbon chain radicals are formed by discharging different gas mixtures in the throat of a pulsed plasma nozzle, either a slit nozzle[22] or pinhole design.[23] For C_6H and C_6D, 0.5% $^{12}C_2H_2$ in He and 0.3% $^{12}C_2D_2$ in He mixtures are used, respectively. An isotopically enriched $^{13}C_2H_2$ (99% purity) gas sample, mixed at 0.13–0.18% in He/Ar (85/15) is used to record fully ^{13}C-substituted $^{13}C_6H$ spectra. A solenoid valve (General Valve, Series 9) on top of the nozzle body controls a high pressure (5–10 bar) gas pulse (roughly of 1 ms duration) that is discharged between ceramically isolated electrodes before expanding into a vacuum, generated by a powerful roots blower system. Typically, 300 to 500 μs long negative high voltage pulses (V/I ~ -750 V / 100 mA) are offered to dissociate the precursor species and to allow molecule formation through collisions in the expanding plasma. In parallel the adiabatic expansion allows for final rotational temperatures in the order of 15 to 25 K.

The output of a pulsed Nd:YAG-pumped dye laser is aligned just below (2–5 mm) and parallel to a 3 cm $\times$ 300 μm slit nozzle, or across the conical jet of a 1.0 mm diameter pinhole. The effective absorption pathlength along the slit or through the pinhole expansion can be further improved by orders of magnitude by positioning the slit nozzle (or pinhole) along the optical axis between two highly reflective mirrors (R > 0.99998) in a cavity ring-down configuration.[24] Typical values for the ring-down time amount to τ = 40 to 100 μs, corresponding to effective path lengths of several kilometers through the plasma. The experiment runs at 10 Hz and precise pulse generators are used to guarantee that gas and discharge pulse as well as ring-down event coincide in time. Typically the average of 10 ring-down events is used for each laser wavelength before being stored as a data point.

The laser bandwidth is about 0.035 cm^{-1}, thus sufficiently narrow to resolve subsequent rovibronic transitions in C_6H that has a rotational constant of the order of 0.045 cm^{-1}, i.e., two lines are separated by about 0.090 cm^{-1}. Wavelength calibration is achieved by recording simultaneously an etalon transmission spectrum (FSR $\sim$ 20.1 GHz) which provides relative frequency markers for correction of any nonlinearity during scanning. An iodine (I_2) spectrum is recorded for absolute wavelength calibration, yielding an overall accuracy of better than 0.02 cm^{-1}.

The use of the slit nozzle leads to nearly Doppler-free spectra due to a collimation effect on the gas pulses emanating from the slit jet expansion perpendicular to the laser beam inside the ring-down cavity. In the case of the pinhole nozzle the contribution of molecules with velocity components along the laser beam path is larger, therewith producing spectral lines with extended Doppler broadening. However, the latter effect can be partially counteracted by mixing Ar in the gas sample, which produces a favorable effect on the spectral linewidth. This advantage is exploited for the recording of $^{13}C_6H$ spectra. The isotopically enriched $^{13}C_2H_2$ was used in combination with the pinhole nozzle which uses up less gas than the slit nozzle. A few of the ^{13}C-containing bands were nevertheless recorded in the slit nozzle configuration.

Obviously, the optical methods used are not mass selective, and spectra contain information from a number of species formed in the plasma, including separate transitions originating from, for example, C_2, C_3, or CH. Also, under similar experimental conditions, long linear[25] and bent chain[26,27] carbon-based molecules are formed in the plasma expansion. While under the presently used plasma expansion conditions the larger molecules are rotationally and vibrationally cooled, typically exhibiting rotational temperatures of $T_{\rm rot} \sim 20$ K and vibrational temperatures of the same values,[17] the diatomic radicals C_2 and CH are detected at elevated temperatures even allowing the detection of C_2 in the metastable $a^3\Pi_u$ state in the $v = 9$ level.[25] It is noted that the resulting rotational temperature can be regulated by changing the nozzle-to-laser-beam distance.[17,23] Further, the plasma chemistry is different under conditions of a conical expansion when a pinhole nozzle is employed, or for a planar expansion in the case of a slit jet configuration. The spectral features associated with C_2 and CH, which in some cases can be assigned to previously identified transitions, overlap and in some cases congest the C_6H features under investigation in the present study. The isolated line features pertaining to C_2 and CH (and possibly other radicals) will be indicated by an asterisk ($*$). In particular, in the energy region higher than $19\,350$ cm^{-1}, with the (0,0) band origin of the $d^3\Pi_g - a^3\Pi_u$ C_2 Swan band at $T_0 = 19\,378.4646(7)$ cm^{-1},[28] the spectra become swamped by a line forest, for which reason no spectra for C_6D and $^{13}C_6H$ will be reported in this range. For C_6H the sequence of vibronic states is presented despite the fact that the spectra are severely contaminated by C_2 lines. With the PGOPHER[29] program and using spec-

troscopic constants from the literature,[28] we can simulate and identify most of the strong C_2 lines originating from the (0,0) and (1,1) Swan bands.

In addition to the spectral features associated with the absorption lines of these diatomic radicals, some of the recorded spectra are overlaid by absorption features of unknown origin, which, due to their isolated nature, may be connected to atomic lines. These features, that will be indicated by hashes (#), are in some cases detected as reduced absorptions, hinting at amplified spontaneous emission or laser-induced fluorescence features. Since we failed to assign those features they will be treated as artifacts in the following. We note here that the presently reported spectra were recorded over a 5-year interval (2010–2015) and a number of bands were fully reproduced using independently produced gas mixtures from which we conclude that these 'artifacts' are not due to measurement issues but are reproducible spectral features associated with atomic or molecular absorption or emission, although unassigned.

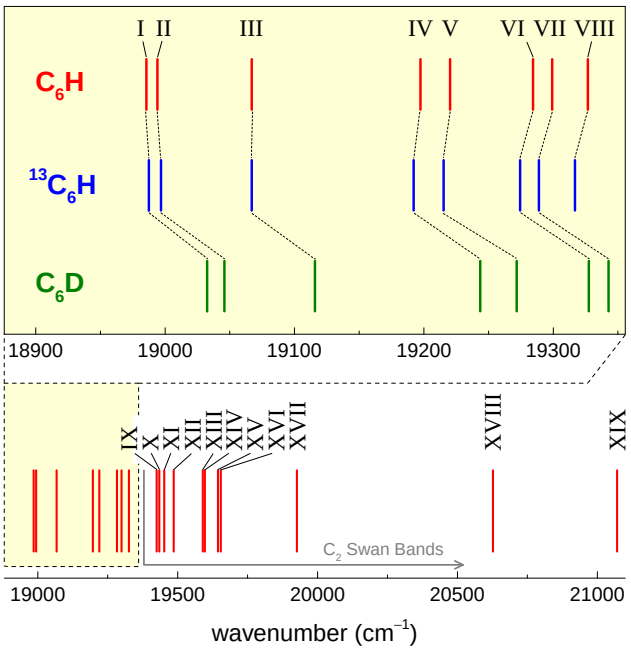

Figure 1: Stick diagram denoting the positions of all the observed bands in the $18\,950 - 21\,100$ cm^{-1} range for C_6H (in red, lower panel). The corresponding bands for $^{13}C_6H$ (blue) and C_6D (green) are shown in the zoomed portion (upper panel) and are connected with dotted lines. The area with overlapping C_2 Swan transitions is indicated.

Results

The survey covers the $18\,950$–$21\,100$ cm^{-1} ($\sim$ 527–473 nm) range and comprises a large number of bands. For each isotopologue, eight individual bands (seven for C_6D) have been unambiguously assigned. In the case of C_6H, eleven additional bands have been recorded that exhibit very different spectral features. The assignments to C_6H, $^{13}C_6H$, and C_6D are based on a rotational analysis of the bands where it is assumed that in the cold jet expansion, the population is only retained in the lowest spin-doublet of the $X^2\Pi$ state for both $^2\Pi_{3/2}$ and $^2\Pi_{1/2}$ components and in the very low lying $\mu^2\Sigma$ Renner-Teller component of the ν_{11} bending vibration. For these ground states, accurate molecular constants are available from microwave data[5–7] except for the $^{13}C_6H$ isotopologue for which the ground state constants were determined optically[17] and via isotopic scaling. The use of the available information allows us to identify the character of the lower state of the bands. As for the assignment of the excited state vibrational levels, this is based on neon matrix spectra[14,15,30] in combination with *ab initio* calculations.[8–11,19]

In Fig. 1 an overview of the band origins of all the observed optical absorption bands is shown for the three species studied here: regular C_6H, $^{13}C_6H$, and C_6D. Connected by dotted lines, the corresponding bands in the zoom-in (upper panel) of Fig. 1 show a similar pattern for each of the three isotopologues. These isotopic shifts further guide in identifying the absorbing species. The labels with Roman numerals I–XIX in the figure correspond with those used in the sections below and in Table 1 and are based on the order at which the bands appear in the overall spectrum. A substantial number of the observed bands has been recorded at rotational resolution and for many of these bands accurate molecular parameters have been derived using PGOPHER. The bands were described either by a $^2\Pi - ^2\Pi$ or a $^2\Sigma - ^2\Sigma$ transition (see below). For the rotational and fine structure analysis, we adopt the effective Hamiltonian of a diatomic molecule, which may be used for transitions in a linear polyatomic molecule such as C_6H. The fitting routine takes ground state values for the rotational constant B'', the centrifugal distortion constant D'', the spin-orbit constant A'', and the spin-rotation constant γ''; these parameters are kept fixed in optimizing the excited state values. With the exception for the origin band (Bands I and II) and for the next vibronic band (Band III), we assume $D' \approx D''$: 1.35×10^{-9} cm^{-1} (C_6H) and 1.2×10^{-9} cm^{-1} ($^{13}C_6H$ and C_6D). As in the plasma jet, particularly, lower lying rotational levels are probed, an independent fit of D' is not possible for the majority of the bands presented here.

The resulting values are summarized in Table 1. For some bands a rotational analysis could not be performed, either due to a poor signal-to-noise ratio, overlapping features from other species, or due to lifetime broadening. For these cases only approximate molecular constants are reported.

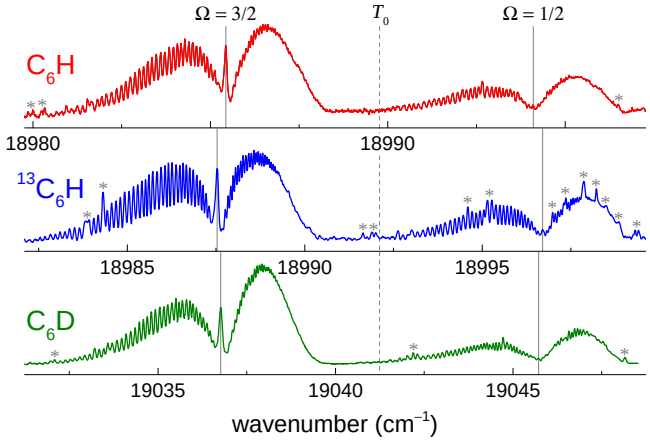

Figure 2: The $B^2\Pi$–$X^2\Pi$ electronic origin band (referred to as Bands I and II) of C_6H, measured with a slit plasma nozzle, with the fully ^{13}C-substituted and the deuterated isotopologue. All three spectra, measured in the slit jet configuration, are plotted here on the same scale with their band origins aligned (denoted by T_0). Peaks marked with an asterisk (∗) are blended transitions from smaller species.

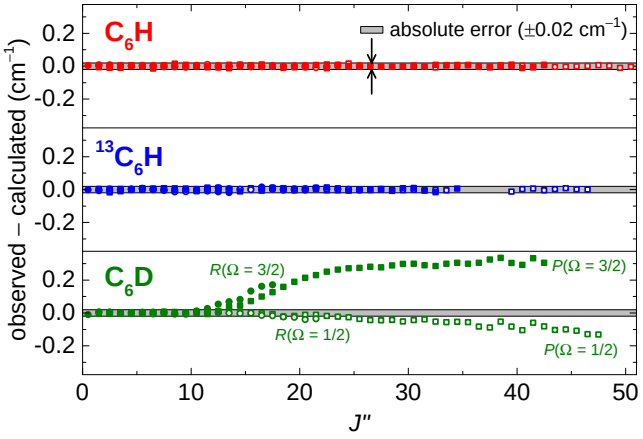

Figure 3: Residuals plotted for each of the observed rotational transitions in the electronic origin band. Squares (□) denote P branch lines and circles (○) to R branch lines, with the filled symbols referring to $\Omega = 3/2$ and open symbols to $\Omega = 1/2$. Notice that for both C_6H and $^{13}C_6H$, residuals fall within the uncertainty margins while in C_6D they deviate for higher J''.

Bands I and II: 0_0^0 $B^2\Pi_\Omega$–$X^2\Pi_\Omega$ origin band

Fully resolved rovibronic spectra of the $B^2\Pi$–$X^2\Pi$ origin band transition have been reported before.[6,17,31] Figure 2 shows the cavity ring-down spectra of C_6H, $^{13}C_6H$, and C_6D. The spectra are repeated for completeness and as an introduction to the interpretation of the other $^2\Pi - {}^2\Pi$ bands presented later.

In each spectrum two spin-orbit components of a band system are shown, corresponding to the (0,0) band origin of the $B^2\Pi_{3/2}$–$X^2\Pi_{3/2}$ (left of T_0) and the $B^2\Pi_{1/2}$–$X^2\Pi_{1/2}$ (right) transition. Each component displays largely rotationally resolved P and R branches. In the $B^2\Pi_{3/2}$–$X^2\Pi_{3/2}$ case, the Q branch is clearly visible; in the $B^2\Pi_{1/2}$–$X^2\Pi_{1/2}$ case it is much harder to discriminate. The two subbands are split by the difference in spin-orbit splitting between the ground and the electronically excited state, $A' - A''$. Depending on whether this number is positive or negative, the $B^2\Pi_{3/2}$–$X^2\Pi_{3/2}$ component is situated to lower or higher energy of the $B^2\Pi_{1/2}$–$X^2\Pi_{1/2}$ component, assuming that both ground state and excited state have a regular or inverted spin-orbit splitting. As the intensity of the Q branch scales with Ω^2, it is clear that the lower energy component corresponds with the $B^2\Pi_{3/2}$–$X^2\Pi_{3/2}$ system.[6] Also, a full rotational analysis (results presented in Table 1) shows that the band gap amounts to roughly $10B$, with B as the rotational constant, instead of $6B$ as typical for the $B^2\Pi_{1/2}$–$X^2\Pi_{1/2}$ band. As a consequence the assignment of the two bands is straightforward and in combination with microwave data[5] the spin-orbit splittings are set as an inverted system with $A'' = -15.04$ cm^{-1} and $A' = -23.69$ cm^{-1}. Based on these numbers and the overall pattern, it is also possible to derive the spin-orbit and rotational temperatures for our plasma settings, yielding 13–22 K.

These findings apply with approximately the same values to all three species. The fitting of the observed spectra is rather straightforward as very precise microwave constants are available to characterize the electronic ground state, but only for the case of C_6H and C_6D.[6] Since there are no ground state constants for the $^{13}C_6H$ species from microwave or infrared spectroscopy, both the upper and the lower energy levels of the $B^2\Pi$–$X^2\Pi$ (0,0) transition are optimized in the fitting,[31] and the resulting ground state molecular constants will be used for the simulation and fitting of the other $^{13}C_6H$ bands.

In previous work, extensive lists with line positions have been given for these bands, and using PGOPHER accurate molecular parameters have been derived for C_6H and C_6D[17] as well as for the ^{13}C-substituted species.[31] Shown in Fig. 3 are the differences between the observed and calculated (o–c) values which are derived from these line lists (see Supporting Information). In comparing the behavior of the residuals for the three molecules, the o–c values of C_6D deviate outside the experimental uncertainty. For $J'' > 15.5$ (10.5) in the $B^2\Pi_{3/2}$–$X^2\Pi_{3/2}$ ($B^2\Pi_{1/2}$–$X^2\Pi_{1/2}$) component, residuals can become an order of magnitude larger than the absolute uncertainty of ±0.02 cm^{-1}. The deviation for the $B^2\Pi_{3/2}$–$X^2\Pi_{3/2}$ component starts early on and goes to a much larger value as compared to that of the $B^2\Pi_{1/2}$–$X^2\Pi_{1/2}$ component. This behavior is indicative of a perturbation of the excited state level structure in C_6D.

DOI: 10.1021/acs.jpca.6b06647

Band III: $\{11\}^1_1$ $\mu^2\Sigma - \mu^2\Sigma$ vibronic band

First among the newly recorded vibronic spectra is the $\{11\}^1_1$ $\mu^2\Sigma - \mu^2\Sigma$ transition of $^{13}C_6H$, highlighted in the middle panel of Fig. 4. While this band exhibits clearly discernible P and R branches, no Q branch is observed, indicative of a $\Sigma - \Sigma$ type of transition, which does not allow for a change of electronic angular momentum and thus, $\Delta J = 0$ is forbidden.[32] For C_6H and C_6D corresponding bands have been identified as originating from the $\{11\}^1_1$ $\mu^2\Sigma - \mu^2\Sigma$ vibronic hot band, and full rotational and Renner-Teller (RT) analyses have been presented previously.[17] Here we use the information from the rotational analysis of C_6H and C_6D to fit the $^{13}C_6H$ line positions. First, a spectral simulation using the C_6H constants (after isotopic scaling) is used to assign the individual $^{13}C_6H$ transitions. These are then included in a fit with PGOPHER using a regular $^2\Sigma - {}^2\Sigma$ Hamiltonian, yielding the $^{13}C_6H$ constants. The resulting simulation is shown in Fig. 4.

Apart from the blended absorption lines from small species, the fit reproduces the experimental spectrum convincingly, including the irregular features in the P branch and the bump in the R branch. We can decompose this fitted curve into two subbands labelled $F_1 - F_1$ and $F_2 - F_2$ to show clearly the doublet P and doublet R band structure. The $F_1 - F_1$ subband gives rise to $P_1(J)$ and $R_1(J)$ branches, and the $F_2 - F_2$ subband to $P_2(J)$ and $R_2(J)$ branches. The overlap of the $P_1(J)$ and $P_2(J)$ branches reproduces the experimentally observed spectral interference, and a more intense $R_2(J)$ compared to the $R_1(J)$ branch produces the step-like phenomenon at 19 068.3 cm^{-1}. The relative intensity of the two subbands also confirms the vibronic assignment since different values for the rotational constants result in different band contours. It is interesting to note that in this way the somewhat irregular appearance of Band III can be fully reproduced. The derived molecular constants are listed in Table 1.

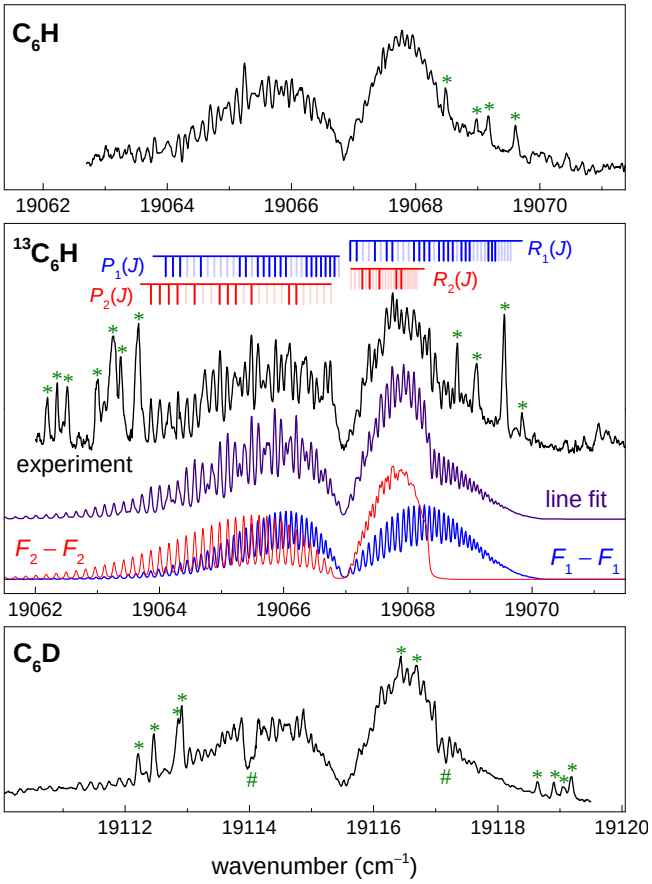

Figure 4: The $\{11\}^1_1$ $\mu^2\Sigma - \mu^2\Sigma$ vibronic band (Band III), for all three isotopologues measured in the slit jet configuration. For each branch, the lines are assigned with heavy tick marks. Blended lines from small species are marked with asterisks (∗). Dips, that are reproduced in independent scans, are present in the C_6D spectrum and are marked with hashes (#). Rotational analyses of C_6H and C_6D spectra have been presented in Ref. [17].

Band IV: $\{10\}^1\{11\}_1$ $\mu^2\Sigma - \mu^2\Sigma$ vibronic band

A well resolved spectrum of this band system (Band IV) is reported for the first time and has been measured for all three isotopologues (Fig. 5). The appearance of the band structure for the three isotopologues is very similar, providing confidence in assigning the three spectra to the same band system. Largely resolved P and R branches are observed at the low and high energy side of an unresolved and structureless feature, more or less at the position where a Q branch might be expected. However, in a simulation it can be shown that these unresolved features are due to the $R_2(J)$ branch of the $F_2 - F_2$ component in a $^2\Sigma - {}^2\Sigma$ band. The intensities of these unresolved features scale with that of the P and R branches and must, therefore, be part of this band system.

The different appearance, compared to Band III, is caused by a larger ratio between the effective spin-rotation constant γ and the effective B rotational constant (see Table 1), causing the lines in the $R_2(J)$ branch to move closer together, forming a band head which is uncommon for low rotational temperatures. This is illustrated in Fig. 5 where the fits of the individual subbands as well as the composite spectrum are shown. Despite these overlapping transitions, it is possible to assign some of the rotational levels and perform a fit. This is because at the low energy side the $P_2(J)$ transitions contribute largely to the intensity, while at the high energy side the $R_1(J)$ branch is the sole contributor to the spectrum. In the experimental spectrum the individual rotational lines are largely resolved and these are well reproduced by the fitted spectrum. This even applies to the overlapping rotational structure in the energy region just at the low energy side of the

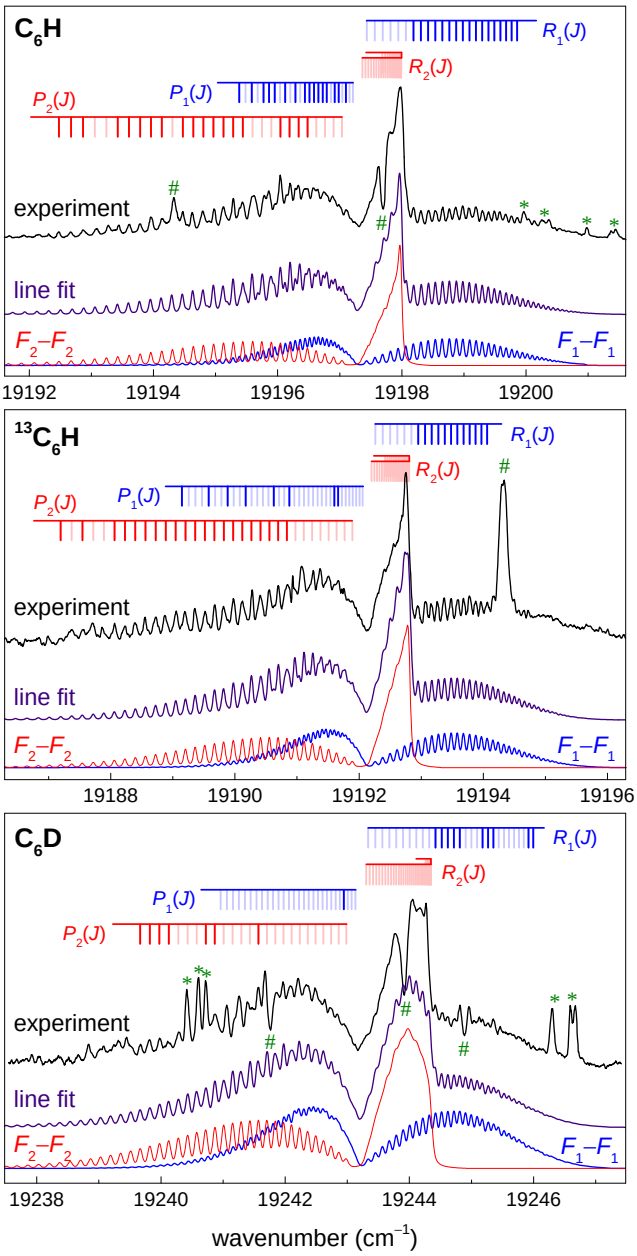

Figure 5: Recording of the $\{10\}^1\{11\}_1\ \mu^2\Sigma - \mu^2\Sigma$ vibronic band (Band IV) for C_6H (upper), $^{13}C_6H$ (middle), and C_6D (lower). Both spectra for C_6H and C_6D were measured using the slit nozzle configuration. For $^{13}C_6H$ the pinhole nozzle configuration was used with an admixture of argon gas to reduce Doppler broadening. Blending absorptions from smaller species are marked with asterisks (∗). For features marked with a hash (#), see text.

$R_2(J)$ band head.

The observed spectra are well reproduced using the corresponding ground state constants derived for Band III, confirming that Band IV originates from the same $\{11\}_1\ \mu^2\Sigma$ state. Also the relative intensities of the subbands $F_1 - F_1$ and $F_2 - F_2$ further support this assignment. It should be noted, though, that for C_6H and C_6D, a narrow depletion in the absorption signal has been found in the $R_2(J)$ band head region that is not reproduced in the fit. Should this be a perturbation in the upper rotational states, a corresponding dip should show up in the P branch, but this is not observed. A simulation of the spectra for C_6H and C_6D including these anomalies, marked by a hash (#), turned out to be impossible. In the same way for $^{13}C_6H$ a strong and broad line shows up around 19194.3 cm^{-1} with unclear origin. Incidentally the strong line in $^{13}C_6H$ coincides with a small peak in the C_6H spectrum, at exactly the same frequency, both marked by a hash (#), again indicative of the same feature of unknown origin; an assignment is not possible at this moment. The molecular constants for this band are collected in Table 1.

Band V: $\{10\}^1\{11\}_1\ \kappa^2\Sigma - \mu^2\Sigma$ vibronic band

Band V (Fig. 6) is another well resolved spectrum with a band contour that is very much alike Band IV which strongly suggests that a similar type of electronic transition ($^2\Sigma\ -^2\ \Sigma$) is taking place. With a number of resolved transitions, a rotational line fit can be performed, yielding the molecular constants as listed in Table 1. The simulations reproduce the lines and the overall contour, although for $^{13}C_6H$ the peak of the central spectral feature is slightly off by $\sim$ 0.2 cm^{-1} to higher energy. The vibrational assignment of Band V in connection with Band IV is described in the Discussion section.

Band VI: $\mu^2\Sigma - \mu^2\Sigma$ vibronic band

The spectra assigned to Band VI and recorded in the slit jet configuration are presented in Fig. 7. At first glance the contour of Band VI is reminiscent of Band III, rather clearly for C_6H and C_6D, pointing to a $^2\Sigma - {}^2\Sigma$ transition. For C_6H, having the best S/N for this band, a fit to the rotational structure is well possible using the ground state constants obtained for the Renner-Teller $\mu^2\Sigma$ ground state. Again the intensity in the R branch is most pronounced and also the intensity drop at 19 285.4 cm^{-1} can be understood as a result of the contribution by the $F_1 - F_1$ and $F_2 - F_2$ subbands. The spectrum for C_6H has a single artifact feature denoted by a hash (#), while the spectra of C_6D and $^{13}C_6H$ are overlaid by multiple artifact features and extra lines associated with small radicals, denoted by asterisks (∗).

Given the low S/N, for the $^{13}C_6H$ and the C_6D spectrum a good line fit is not possible for molecular constants isotopically scaled from the main C_6H isotopologue. Moreover, anomalous band features make it harder to identify and assign rotational lines. The lack of individually resolved rotational transitions necessitates a contour simulation using the known ground state values and tuning the excited state parameters together with the rotational temperature until the overall shape of the band is matched. Clearly, results obtained

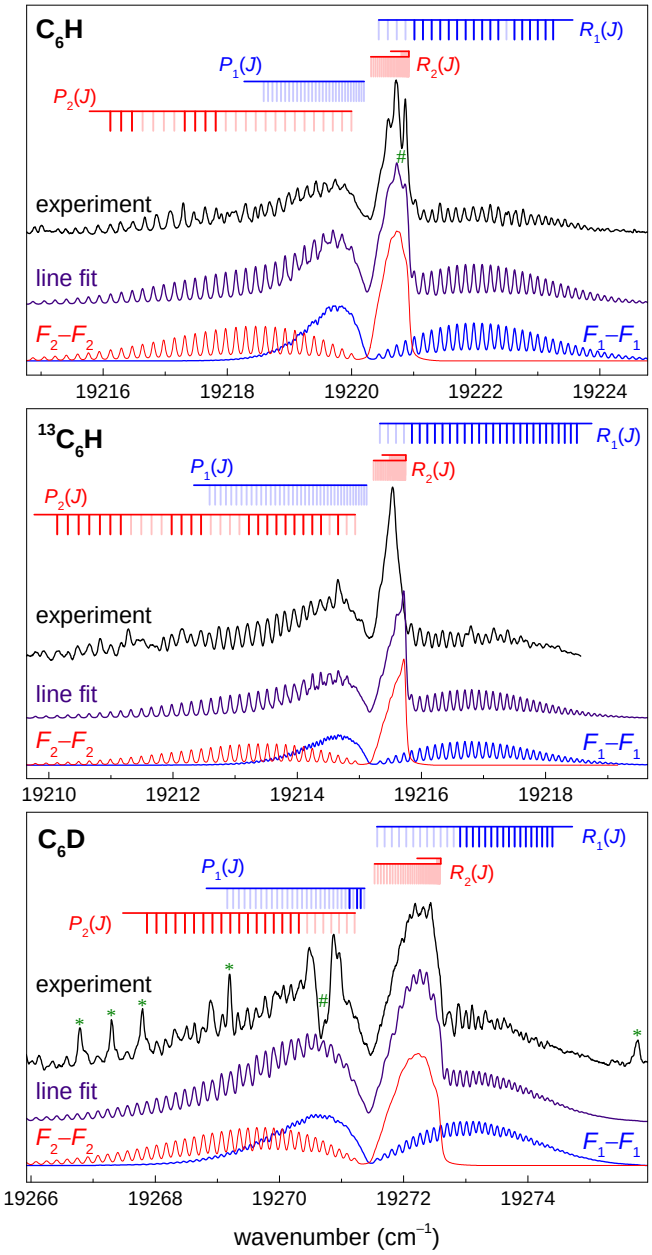

Figure 6: Band V assigned as the $\{10\}^1\{11\}_1\ \kappa^2\Sigma - \mu^2\Sigma$ transition. Again, distinct dips (marked with #) show up in the spectra which cannot be accounted for in the rotational line fit.

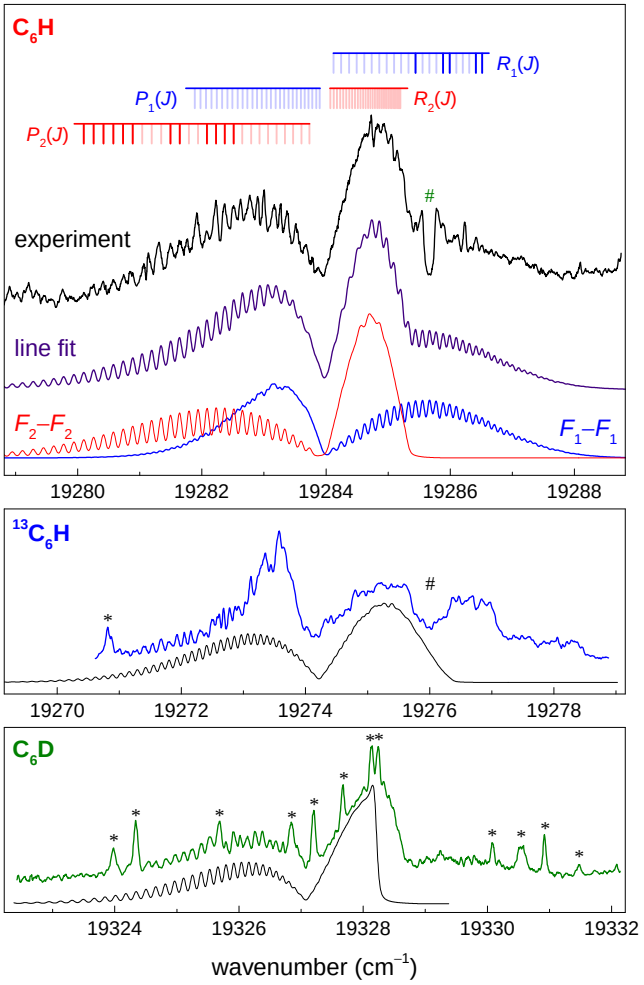

Figure 7: Band VI assigned as a $^2\Sigma - {}^2\Sigma$ transition. All three spectra were recorded using the slit nozzle configuration. Shown in the upper panel is a rotational line fit done for C_6H with the two band components. For $^{13}C_6H$ and C_6D a band contour simulation (in black) was performed. Features denoted by asterisks (∗) and hashes (#) are discussed in the main text.

using this procedure will not be as precise as the results from a line fit. So as an additional criterion to verify the correct simulation of the spectrum, the spacing between individual (but unassignable) rotational lines has been matched, typically in the P branch.

The spectrum for C_6D is overlaid by a number of sharp lines (marked by ∗). If this is taken into account, the contour fit yields a reasonable simulation of the observed spectrum, although the sharp drop in the simulated intensity of the R branch is not clearly reproduced.

Of the three spectra, the $^{13}C_6H$ spectrum exhibits the most severe anomalies which makes it less straightforward to obtain a proper band contour simulation. The increased intensity in the P branch near $19\,273.5\ \mathrm{cm}^{-1}$ might be associated by the spectral lines of small radicals contributing to the intensity, although no sharp and distinct lines are visible. In the R branch of $^{13}C_6H$ a double broad feature appears which could be due to an artifact dip (marked by #) or it may well be that the second feature is caused by a different species since it is rather outside the simulated intensity pattern. In any case the observed spectrum deviates quite distinctively from a constructed band contour as shown in the figure, and so the resulting constants should be treated with care.

The molecular constants obtained from a fit of the

C_6H spectrum and a band contour simulation for C_6D and $^{13}C_6H$ are listed in Table 1.

Band VII: $B^2\Pi_\Omega$–$X^2\Pi_\Omega$ vibronic band

Spectra of Band VII, recorded in the slit jet configuration for all three isotopologues, are displayed in Fig. 8. The overall shape of the band structures for the three isotopologues is similar, which forms the basis for assigning these spectral features to the same band. In the band gap region between the P and R branches a clear peak reminiscent of a typical Q branch is found. In the spectra for C_6H and C_6D some additional lines associated with small radicals (marked with $*$) are visible as well, and their shape is somewhat similar to the Q branch feature. However, because these extra lines do not occur in the spectrum for $^{13}C_6H$ and the location of the Q branch is in all cases at the appropriate frequency, the identification of a Q branch feature is unambiguous. Hence Band VII is assigned as $^2\Pi - {}^2\Pi$.

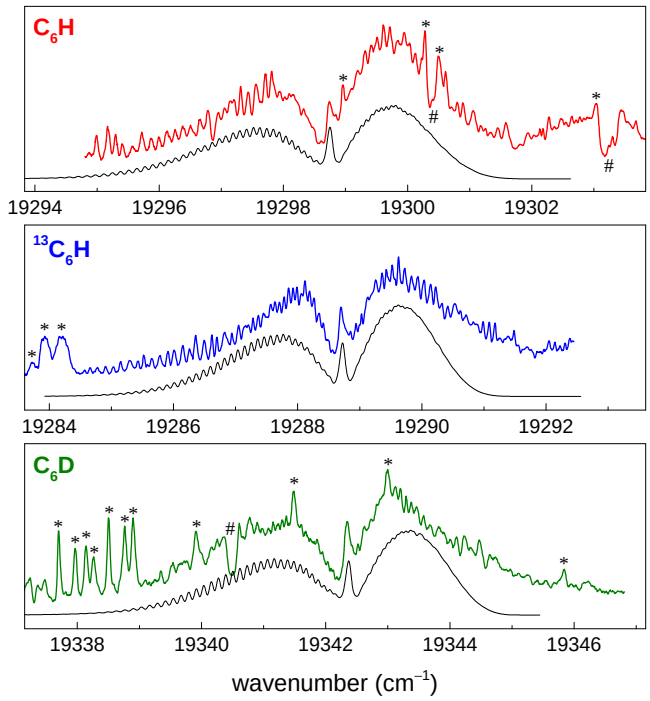

Figure 8: Spectral recordings of Band VII, here identified as a $^2\Pi - {}^2\Pi$ transition. All spectra were recorded using the slit nozzle configuration. Again blended lines ($*$) and dips (#) are visible in the spectrum. Simulated band contours are shown in black.

As was discussed in previous studies of the $^2\Pi - {}^2\Pi$ band origin transition in C_6H,[6] the Q branch is most visible for the $\Omega = 3/2$ spin-orbit component, while it is hardly visible for $\Omega = 1/2$; this intensity relationship is exemplified in the origin band (Fig. 2). Detailed inspection of the recorded Q branches of Band VII for all isotopologues shows that all three are somewhat blue-degraded, unlike in the case of the origin band, where the Q branches are red-degraded. Such a line shape is difficult to explain. A possible rationale is that the two spin-orbit components of the transition, hence $^2\Pi_{3/2} - {}^2\Pi_{3/2}$ and $^2\Pi_{1/2} - {}^2\Pi_{1/2}$, are overlapped with each other to some extent, which further implies that for this transition, $A' \approx A''$. A similar situation applies to other species, like HC_6H^+ and HC_8H^+, where transitions starting from both spin-orbit components coincide and differences are only visible for higher rotational temperatures.[33] In principle, it is also possible that A'' increases, and for a similar spin-orbit temperature, this means that the population in the $\Omega = 1/2$ state decreases. This is not expected, as the ground state splitting should be the same for all $^2\Pi - {}^2\Pi$ transitions studied here. The constructed contours, shown in black in Fig. 8, are based on this assumption. In all three cases the observed spectra are reasonably well reproduced in the contour fits and the underlying molecular constants are listed in Table 1.

Band VIII: $B^2\Pi_{3/2}$–$X^2\Pi_{3/2}$ vibronic band

Figure 9 displays the spectra of Band VIII recorded for C_6H and $^{13}C_6H$. Band VIII was not recorded for C_6D since in the energy region beyond $\sim 19\,350\ \mathrm{cm}^{-1}$, where this band is expected (see also Fig. 1), the spectra are covered by very strong absorptions from the C_2 Swan bands.

Again, as in the case of Band VII, the spectra are characterized by the presence of a pronounced Q branch, the reason for assigning this band to a $^2\Pi - {}^2\Pi$ type transition. This time, the Q branch lies more to the P branch side, and the line shape of the Q branch is red-degraded, which is an indicator for a $^2\Pi_{3/2} - {}^2\Pi_{3/2}$ transition. Indeed both spectra for C_6H and $^{13}C_6H$ can be well reproduced by a contour simulation. Values obtained from the contour simulation are listed in Table 1.

Bands IX and X: $B^2\Pi_\Omega$–$X^2\Pi_\Omega$ vibronic band

In the narrow frequency window at $19\,420 - 19\,440\ \mathrm{cm}^{-1}$ two more absorption bands are found that are heavily overlaid by strong resonances from C_2. Using molecular constants from the literature,[28] these blending peaks can be attributed to the (0,0) origin band of the Swan system of C_2. This simulation and together with the spectra recorded in the slit jet configuration are displayed in Fig. 10. The observed bands (Bands IX and X) have the shape of a $^2\Pi_\Omega - {}^2\Pi_\Omega$ pair: very similar to bands I and II. Band IX has a narrow resonance at $19\,424.9\ \mathrm{cm}^{-1}$, which is not reproduced by a Swan band line like most of the other sharp resonances observed. This resonance, identified as a Q branch, is centered in between apparent P and R branch features. Following the argument, as for Bands I and II, that the $\Omega = 3/2$ component exhibits a much stronger Q branch than the $\Omega = 1/2$ component, a contour fit can

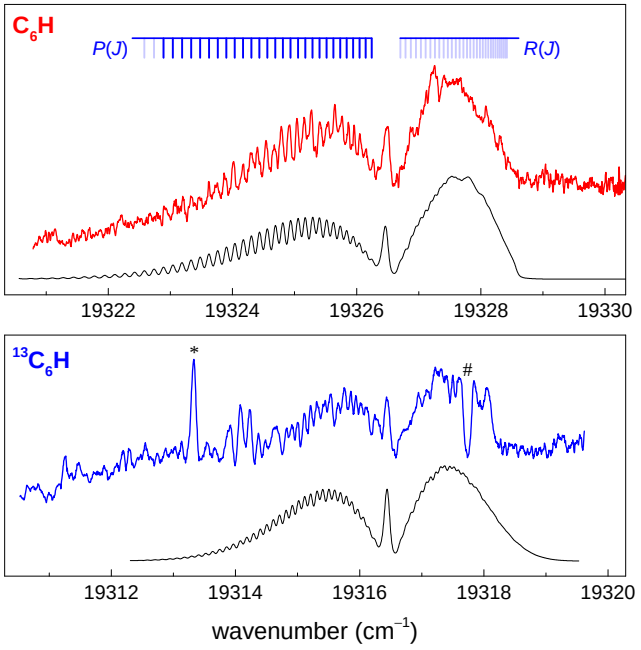

Figure 9: Spectra for Band VIII, assigned as the $\{9\}_0^1$ $B^2\Pi_{3/2}$–$X^2\Pi_{3/2}$ transition, recorded for C_6H in the slit nozzle configuration and for $^{13}C_6H$ in the pinhole nozzle configuration. Simulated band contours are shown in black.

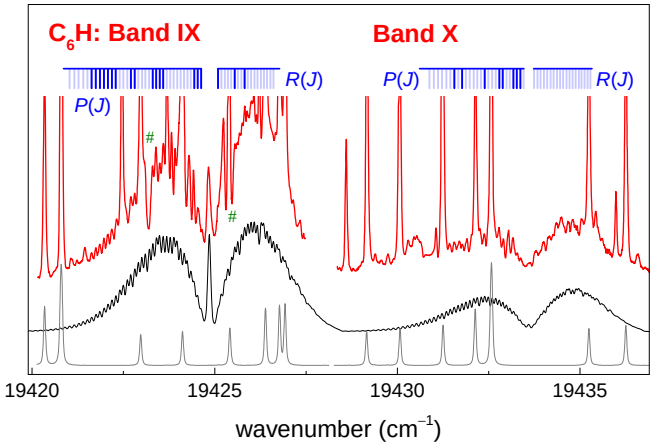

Figure 10: Bands IX and X of C_6H measured in a slit jet plasma configuration and a rotational line fit for a $^2\Pi_\Omega - {}^2\Pi_\Omega$ band for both $\Omega = 3/2$ and $1/2$ components. At the bottom of the figure a simulated spectrum of overlapping C_2 Swan transitions is plotted.

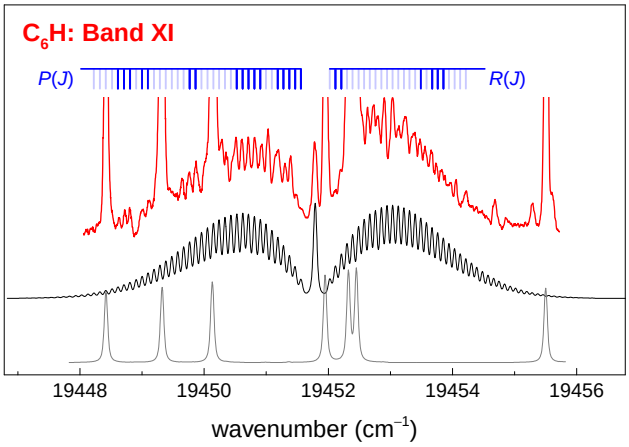

Figure 11: Recording of Band XI of C_6H in a slit jet plasma configuration and a rotational line fit assuming a $^2\Pi_{3/2} - {}^2\Pi_{3/2}$ transition.

be produced for the combined $^2\Pi_\Omega$–$^2\Pi_\Omega$ bands using the ground state molecular constants. The agreement of the excited state spin-orbit constant A' with that of the band origin provides confidence for a positive assignment of these bands. It is noted that these bands were presented previously in a PhD-thesis by Denisov [34] employing cavity ring-down spectroscopy, where the bands were also assigned as a $^2\Pi_\Omega - {}^2\Pi_\Omega$ pair. Similarly as in the previously presented vibronic bands, dips show up in the spectra which cannot be reproduced in a fit.

Band XI: $B^2\Pi_{3/2}$–$X^2\Pi_{3/2}$ vibronic band

A recording of Band XI, presented in Fig. 11, is assigned as $^2\Pi_{3/2} - {}^2\Pi_{3/2}$ due to the presence of a Q branch. Again the spectrum in this energy range is overlaid by strong resonances due to C_2 Swan (0,0) band absorption, but the prominent absorption feature at $19\,451.8$ cm^{-1} does not coincide with a predicted C_2 line, and is therefore identified as the Q branch. A number of well-resolved rotational lines in the P and R branches allows for a fit yielding a rotational constant that is indicative of C_6H (see Table 1). The associated $^2\Pi_{1/2} - {}^2\Pi_{1/2}$ spin-orbit component could not be observed.

Band XII: $^2\Sigma - {}^2\Sigma$ vibronic band

Figure 12 shows a recording of a band centered at $19\,486$ cm^{-1}. In a previous study this band feature was associated to the $^2A''$–X^2A'' electronic transition of the $C_4H_4^+$ cation, [35] while in another study, it was identified as a $^3\Sigma^-$–$X^3\Sigma^-$ transition of the C_6H^+ cation. [21] Because the spectrum is overlaid by a number of strong and sharp C_2 Swan transitions, particularly in the region where a Q branch of a possible $^2\Pi_{3/2}$–$^2\Pi_{3/2}$ transition of C_6H may be expected, an unambiguous assignment of this band is difficult. Several band contours were simulated, and by imposing a transition of $^2\Sigma$–$^2\Sigma$ symmetry and keeping the ground state fixed at values for the $\mu^2\Sigma$, Band XII can be well reproduced with excited state constants matching those of C_6H. The fact that the observed interference between simulated P branches for both $F_1 - F_1$ and $F_2 - F_2$ subbands at $\sim 19\,484.6$ cm^{-1} is reproduced in the simulated spectrum lends credit to the assignment of this band to a

$^2\Sigma - {}^2\Sigma$ feature and to assign the C_6H molecule as its carrier. It is interesting to note that the distinctive dip in the R branch at $19\,487.6$ cm^{-1} in Fig. 12, indicated by #, was also observed in the aforementioned studies.[21,35] This again demonstrates that these features of decreased absorption are not just artifact features.

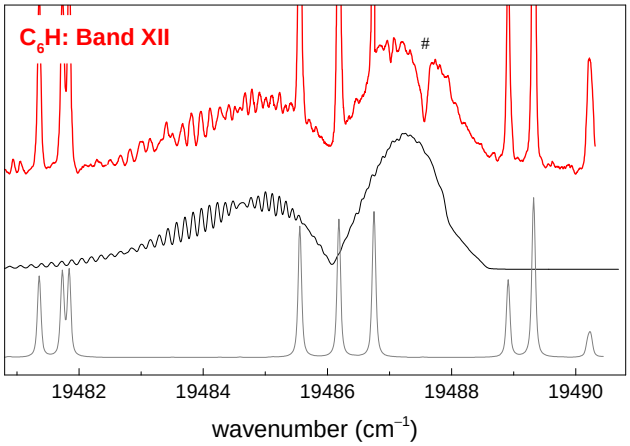

Figure 12: Bands XII of C_6H measured in the slit plasma nozzle configuration. A simulated contour spectrum of a $^2\Sigma - {}^2\Sigma$ transition is plotted in black. The sharp absorption features can be identified as C_2 Swan band lines for bands (0,0) and (1,1) bands (in gray).

Bands XIII and XIV: $B^2\Pi_\Omega$–$X^2\Pi_\Omega$ vibronic band

In the frequency range $19\,587 - 19\,600$ cm^{-1} another composite band feature has been observed which again is heavily overlaid by sharp C_2 (0,0) and (1,1) Swan band transitions. The spectrum (Bands XIII and XIV), presented in Fig. 13, displays the appearance of a $^2\Pi_\Omega - {}^2\Pi_\Omega$ pair. Like for the other $^2\Pi_\Omega - {}^2\Pi_\Omega$ pairs the $\Omega = 3/2$ component (Band XIV) exhibits an identifiable Q branch visible at $\sim 19\,596.5$ cm^{-1}, while the other subband feature (Band XIII) does not display such a pronounced Q branch. However, at this location a weak C_2 line is predicted in the simulation, so the assignment of the C_6H bands remains tentative. In addition the order of the spin-orbit components in the putative $^2\Pi$-doublet is reversed, i.e., $\Omega = 1/2$ falls at lower energies than the $\Omega = 3/2$ component. The molecular constants used for producing the simulated spectrum for the corresponding C_6H features are listed in Table 1.

Bands XV and XVI: $\{6\}_0^1\ ^2\Pi_\Omega - {}^2\Pi_\Omega$ vibronic band

In the frequency range $19\,638 - 19\,656$ cm^{-1} two sequential bands have been observed for C_6H in the slit jet discharge expansion. The spectrum, displayed in Fig. 14, is of low signal-to-noise and overlaid with pronounced sharp resonances due to C_2 Swan band lines. By itself the identification of the features remains somewhat unclear, in particular since the intensity of the $^2\Pi_{1/2} - {}^2\Pi_{1/2}$ component exhibits about the same intensity as the $^2\Pi_{3/2} - {}^2\Pi_{3/2}$ component. Additional measurements using the pinhole configuration and detecting these bands downstream the plasma expansion show that the intensity of the $^2\Pi_{1/2} - {}^2\Pi_{1/2}$ component did not drop in a similar fashion as that of the $^2\Pi_{1/2} - {}^2\Pi_{1/2}$ component of the origin band, as shown in Ref. [17]. The same features were also observed in the hollow cathode discharge experiment[16] and there they were assigned to a $\{6\}_0^1\ ^2\Pi_\Omega - {}^2\Pi_\Omega$ transition, based on a comparison with matrix data. From a contour simulation of the spectrum it follows that both subbands, pertaining to $\Omega = 3/2$ and $\Omega = 1/2$ components, can be well reproduced. This provides support for a definitive assignment of Bands XV and XVI to $6_0^1\ ^2\Pi_\Omega - {}^2\Pi_\Omega$ in C_6H.

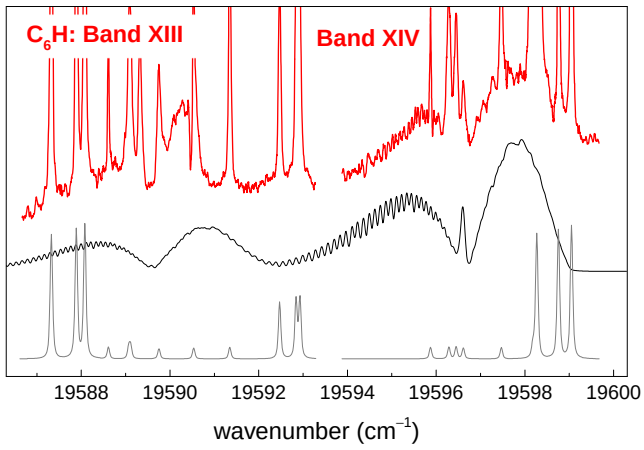

Figure 13: Bands XIII and XIV of C_6H measured in the slit plasma jet configuration with a simulated spectrum based on a $^2\Pi_\Omega - {}^2\Pi_\Omega$ pair with the $\Omega = 1/2$ component at lower energies. The sharp and intense absorption peaks arise from C_2 $(0,0)$ and $(1,1)$ Swan bands (in gray).

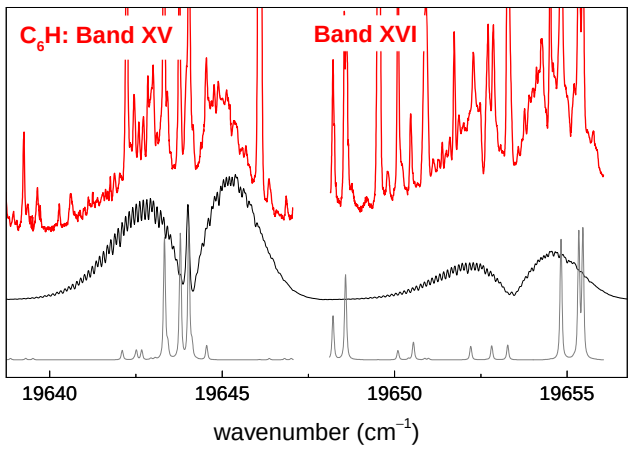

Figure 14: Bands XV and XVI of C_6H measured with a slit plasma nozzle. The blended absorption peaks arise from C_2 $(0,0)$ and $(1,1)$ Swan bands (in gray).

Band XVII: $B^2\Pi_\Omega - X^2\Pi_\Omega$ vibronic band

The band system in the frequency range 19 922 – 19 930 cm^{-1}, displayed in Fig. 15, is of low quality in terms of signal-to-noise and coverage with sharp resonances associated with C_2. The assignment of this feature is very tentative: the central and rather narrow peak at 19 926.7 cm^{-1} might be considered as a Q branch and indicative of a $^2\Pi_{3/2} - {}^2\Pi_{3/2}$ component. But using a similar argument as with Band VII, based on the position of the Q branch, the spectrum can be simulated by superimposing the two spin-orbit components. Only rough estimates of the T_0, B', and A' constants can be given on the basis of a contour analysis, and the corresponding values are listed in Table 1.

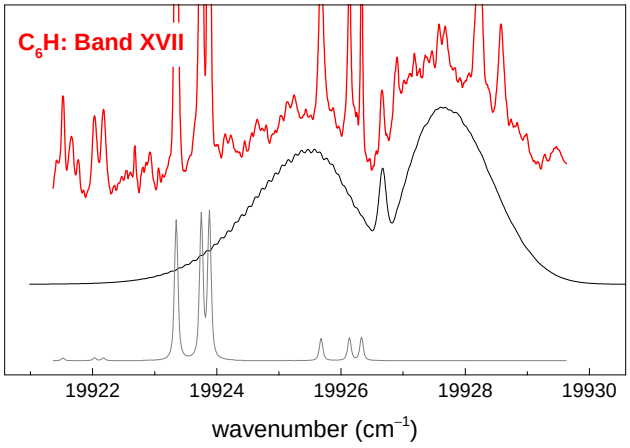

Figure 15: Band XVII of C_6H measured with in the slit jet plasma configuration and a simulation based on a $^2\Pi_\Omega - {}^2\Pi_\Omega$ band type. The narrow absorption peaks arise from C_2 $(0,0)$ and $(1,1)$ Swan bands.

Bands XVIII and XIX

Finally, in the highest energy region investigated in the present study, in the frequency range above 20 000 cm^{-1}, two bands have been observed, which are shown in Fig. 16. Despite the two bands having been measured with a slit plasma nozzle, individual rotational lines of C_6H could not be resolved. The broadening is effective to the extent that the $^2\Pi_{3/2}$ and $^2\Pi_{1/2}$ components are somewhat overlapped, without a distinct Q branch visible. Moreover, the spectra, in particular for Band XVIII, are overlaid by a congested forest of narrow resonances. Assuming a rotational temperature of $\sim$ 22 K, and fixing the ground state constants to those of the $^2\Pi$ ground state of C_6H, a band contour simulation can be produced yielding the molecular constants listed in Table 1.

Discussion

In the present study 19 vibronic (sub)bands pertaining to the $B^2\Pi - X^2\Pi$ electronic system of the C_6H molecule have been observed. For the C_6D isotopologue the seven lowest energy bands have been observed and for $^{13}C_6H$ the eight lowest bands. From the fitting of the recorded spectra, values are derived for the band origins T_0, effective rotational constants $B_{\rm eff}$, effective spin-rotation constants $\gamma_{\rm eff}$, and, for the case of $^2\Pi$ vibronic states, a spin-orbit coupling constant $A_{\rm SO}$. For some of the bands, clearly rotationally resolved spectra have been measured and in these cases a fit has been made comparing individual line positions (see Supporting Information for the line lists). In some additional cases spectra are unresolved or strongly overlaid with narrow spectral features belonging to CH and C_2 radical species. In such cases only a band contour simulation has been produced, for which the uncertainty on the derived spectroscopic parameters is larger.

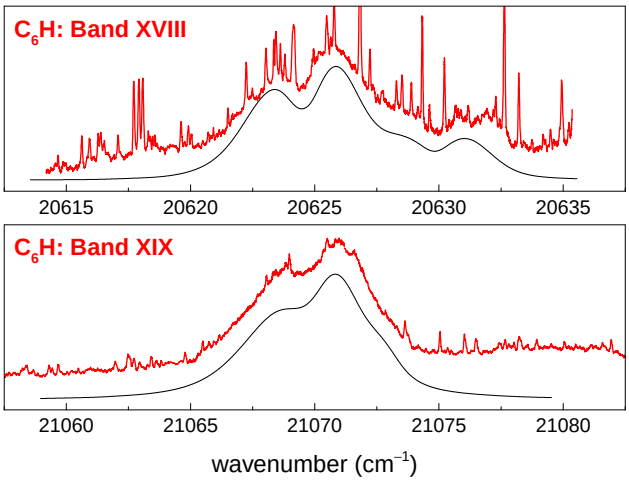

Figure 16: Bands XVIII and XIX of C_6H measured with a slit plasma nozzle and a contour simulation of the spectrum (in black). Note that the wavenumber axis is wider than in the previous figures.

All the bands investigated are connected to an electronic transition of $^2\Pi - {}^2\Pi$ character. If the C_6H molecule were to remain linear in ground and excited state levels then the vibronic absorption bands could all be described as $^2\Pi - {}^2\Pi$ transitions in a diatomic molecule. Even if both $^2\Pi$ states would fit a Hund's case(b) description this would remain the case.[36] If however the spin-orbit splitting in a $^2\Pi$ state becomes appreciable, then the bending vibrations couple to the electronic motion, giving rise to doubly degenerate structures and bands that appear as $^2\Sigma - {}^2\Sigma$ transitions — a phenomenon known as the Renner-Teller (RT) effect. This holds for the case of a single bending vibration. For the non-degenerate stretching vibrations, this is not the case and the electronic absorption bands retain the character of a $^2\Pi - {}^2\Pi$ transition. The same holds for a combination of two degenerate bending vibrations that will also display the character of a $^2\Pi - {}^2\Pi$

transition.

The C_6H molecule is the first member of the C_nH series to be linear in the $X^2\Pi$ ground state, in contrast to the smaller chains like C_4H exhibiting a $^2\Sigma^+$ ground state. This was shown in electronic structure calculations[19,37] and found to be consistent with radio astronomical observations.[2] C_6H is also linear in the vibrationless $B^2\Pi$ excited state as is derived from the gas-phase observation of the $B^2\Pi$–$X^2\Pi$ origin band spectrum.[6] It has 16 vibrational modes, of which there are 5 doubly degenerate bending modes (in the two perpendicular planes containing the molecular axis) and 6 non-degenerate stretching modes. Four different *ab initio* studies have been reported that calculated the non-degenerate stretching modes along the linear axis of the C_6H backbone.[8–11] The calculated eigen frequencies of the fundamental modes, as listed in Table 2, are in reasonable agreement with each other. Two of the cited works on *ab initio* calculations[9,10] also include results on the five doubly degenerate bending modes. Energies of the degenerate modes were calculated to exhibit mode frequencies of $100 - 600$ cm^{-1}, while the energies of the non-degenerate modes fall in the range $600 - 3\,500$ cm^{-1}.

Table 2: The calculated eigen frequencies of the six non-degenerate stretching modes of C_6H as in the four reported *ab initio* studies[8–11] together with the vibrational frequencies derived from the observed gas-phase vibronic spectrum. The observed frequency at $1\,953.4$ cm^{-1} (marked by an $*$) is taken from Ref. [11]. All values in cm^{-1}.

Mode	Doyle 1991[11]	Liu 1992[8]	Brown 1999[9]	Cao 2001[10]	Observed
ν_1	3 659.1	3 609.0	3 448	3 457	
ν_2	2 436.7	2 197.8	2 109	2 137	1 953.4*
ν_3	2 336.0	2 139.6	2 080	2 105	2 080.8
ν_4	2 092.0	1 974.5	1 872	1 895	1 637.4
ν_5	1 213.0	1 201.8	1 210	1 224	
ν_6	653.9	638.5	642	650	658.9

In Fig. 17 the fundamental non-degenerate eigen modes are drawn in the geometry of the C_6H molecule, including calculated bond lengths.[8,9] The highest frequency mode, ν_1, has the typical frequency of a C–H stretching mode and is assigned as such. The three subsequent modes, ν_2, ν_3, and ν_4, in order of decreasing frequency, are associated with the C≡C triple bonds (Fig. 17) where the highest frequency is assigned to the mode with the shortest bond length among the three. The two lowest frequencies, ν_5 and ν_6, are associated with the vibrational motion centered on the C–C single bonds.

These calculations are taken as the basis for assigning the recorded vibronic bands. It should be noted that all four *ab initio* calculations were performed for the ground state electronic configuration, and that we assume the vibrational level structure of the $B^2\Pi$ excited state to reproduce that of the ground state. This is, of course, a rather strong but common assumption. It is

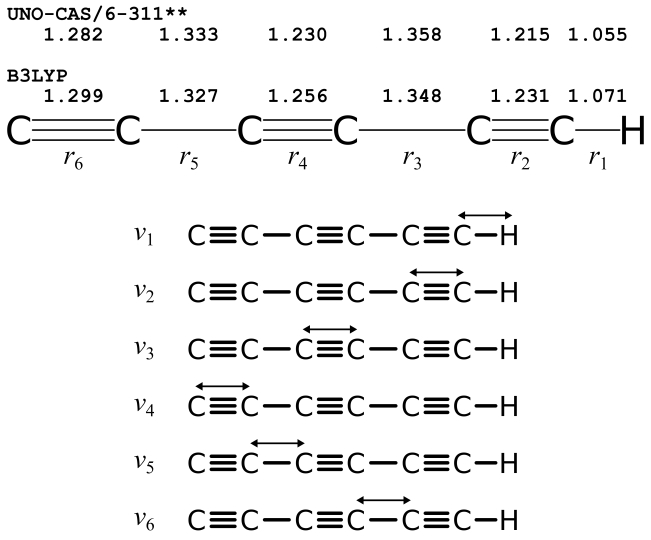

Figure 17: The geometry of the C_6H molecule, adopted from the UNO-CAS/6-311** calculations in Ref. [8] and from the more recent B3LYP calculations in Ref. [9]. Bond lengths (in Å) are exaggerated to emphasize their differences. Also shown are the six fundamental non-degenerate eigen modes where double arrows indicate on which bond the stretching vibration primarily occurs.

noted further that in the study of Brown et al.,[9] ambiguity arises on the identification of the infrared mode observed in the ground state of C_6H at $1\,953.4$ cm^{-1},[11] which is assigned as ν_3 in one of their tables. In another table in the same paper, they still assign this mode to ν_3 but they list a calculated frequency of $2\,109$ cm^{-1}, which corresponds to ν_2 in their previous table. In any case, this IR-absorption is identified as the C≡C stretching vibration next to the C–H bond (r_2 in Fig. 17). In addition, in the photodetachment study by Taylor et al.[18] a vibrational mode at $2\,202$ cm^{-1} was deduced, which however is associated with a low-lying electronic state of $^2\Sigma^+$ symmetry.[19] While the two bands mentioned pertain to the $X^2\Pi$ and $A^2\Sigma^+$ states, in the matrix studies two bands were observed at $21\,645$ cm^{-1} and $22\,517$ cm^{-1}, corresponding to vibrational excitations of $2\,791$ cm^{-1} and $3\,664$ cm^{-1} in the $B^2\Pi$ state. These bands were tentatively assigned as $\nu_3 + \nu_6$ and $\nu_3 + \nu_5$ combination bands,[15] while based on the consistent *ab initio* calculations[8–11] the higher frequency band might also be associated with ν_1.

All observed bands originate from the ground vibrational level, starting from the lowest lying $X^2\Pi_{3/2}$ level, or the $X^2\Pi_{1/2}$ spin-orbit component which is excited by ~ 15.0 cm^{-1}, or from the $\mu^2\Sigma$ component of the RT manifold, which is at an excitation energy of 10.7 ± 0.5 cm^{-1} above the ground level ($X^2\Pi_{3/2}$).[17] The $\mu^2\Sigma$ component is associated with the lowest $\nu_{11} = 1$ bending vibration

in the electronic ground state, which vibronically couples to produce a pair of $^2\Sigma$ states, referred to as a lower $\mu^2\Sigma$ component and a higher lying $\kappa^2\Sigma$ component. This $\kappa^2\Sigma$ component has not yet been observed spectroscopically. Also a pair composed of the $^2\Delta_{5/2}$ and $^2\Delta_{3/2}$ levels follows from the RT coupling, excited at ~ 50 cm^{-1}, which has been observed for C_6H in a microwave study.[7] In the present study no signature of this $^2\Delta$ pair can be identified.

From a spectroscopic analysis of the rovibronic bands and their treatment in the previous section it appears that all bands can be described either by a $^2\Pi - ^2\Pi$ or a $^2\Sigma - ^2\Sigma$ type transition. In the following, all available data are merged with the aim to assign the observed bands to the vibronic level structure of the $B^2\Pi$ state.

The $^2\Pi$ levels

In all cases the bands connected to $^2\Pi - ^2\Pi$ character display the characteristic spin-orbit splitting with $A'' \approx -15$ cm^{-1} for the C_6H and C_6D isotopologues, hence yielding an inverted spin-orbit level ordering between $^2\Pi_{3/2}$ and $^2\Pi_{1/2}$. As discussed previously,[31] the ground state spin-orbit splitting for $^{13}C_6H$ is $A'' \approx -12$ cm^{-1}. In all the fits and band contour simulations the ground state spin-orbit constants have been kept fixed at these values. The spin-orbit structure of the $B^2\Pi$–$X^2\Pi$ (0,0) origin bands of C_6H and C_6D was discussed in earlier studies[6] and yielded an excited state spin-orbit constant of $A' \approx -24$ cm^{-1}. The value for $^{13}C_6H$ of $A' \approx -21$ cm^{-1} can be considered consistent.[31]

The spectra of the $^2\Pi - ^2\Pi$ bands are compared with observations from matrix isolation data, which bear the advantage that a mass-analyzer stage selects the ionized radical species before depositing in a matrix. In this way the matrix data provide an additional constraint that can be used to identify the carriers of the bands discussed here. For C_6H such studies were typically performed in neon matrices cooled to 5 K, where only the $^2\Pi$ ground state was populated.[14,15] In these matrix studies, no excitations associated with the Renner-Teller ν_{11} bending mode were observed, thus creating another helpful selection criterion. Furthermore, several band features, observed in the matrix spectra, were assigned to vibrational modes in the electronically excited C_6H molecule, from a comparison with calculated fundamental frequencies for the electronic ground state of the molecule as available at the time.[8,9] Besides the 0_0^0 origin band of the $B^2\Pi$–$X^2\Pi$ system, three additional non-degenerate modes were observed at vibrational excitation energies of 2 080.8 cm^{-1}, 1 637.4 cm^{-1}, and 658.9 cm^{-1}. These stretching vibrations generate a $^2\Pi - ^2\Pi$ type transition as is clearly observed in the spectra. Of importance for the present analysis is that the matrix shift for the 0_0^0 origin band amounts to -136 cm^{-1}. A typical finding from matrix isolation spectroscopy is that matrix shifts tend to be constants for vibronic structures within a few cm^{-1}. This forms another ingredient for identifying bands.

The spectra of Bands XV and XVI, for which both $^2\Pi_{3/2} - ^2\Pi_{3/2}$ and $^2\Pi_{1/2} - ^2\Pi_{1/2}$ components were observed for C_6H, can be unambiguously assigned to a $^2\Pi - ^2\Pi$ doublet for a number of reasons, even though the spectrum is heavily contaminated. This band was observed in the matrix study[15] exhibiting a matrix shift of -137 cm^{-1} with respect to the present measurement as well as to the shift observed in a lower resolution gas-phase discharge spectrum.[16] The present study yields an excited state spin-orbit constant of $A' = -24.4$ cm^{-1}, which is consistent with that of the origin band. We follow the assignment as in previous studies to match the two components of this band to the lowest non-degenerate vibration, the ν_6 mode, which derives its energy from the vibrational motion of a C–C single bond in the molecule (cf. Fig. 17). It is noted, however, that the intensity ratio between the $^2\Pi_{3/2} - ^2\Pi_{3/2}$ and the $^2\Pi_{1/2} - ^2\Pi_{1/2}$ spin-orbit components behaves somewhat irregularly (see the Results section for Bands XV and XVI).

In a similar way, the bands observed for C_6H in the higher energy region (Bands XVIII and XIX) can be well reproduced by a $^2\Pi - ^2\Pi$ doublet with excited state spin-orbit values of $A' = -20.3$ cm^{-1} and $A' = -16.8$ cm^{-1}, which are in good agreement with the A' spin-orbit constant for the vibrationless origin band. Comparison of the present gas-phase band origins with matrix data yields matrix shifts ~ 133 and ~ 142 cm^{-1}, in good agreement with the typical matrix shift as measured for the 0_0^0 origin band. In previous matrix isolation studies[14,15] these bands were assigned to ν_5 and ν_3 modes from a comparison with the then available *ab initio* data.[8] In the later calculations[9,10] the ν_3 mode is shifted to lower frequencies, which is indeed in agreement with the present observation of $\Delta\nu = 2\,080.8$ cm^{-1}. For the assignment of the band observed at $\Delta\nu = 1\,637.4$ cm^{-1}, the situation is less clear. In view of the most recent calculations this band matches better with the ν_4 mode, than with the earlier identification as ν_5.[15] Hence we keep this assignment as tentative at ν_4.

The observed spectra (see Fig. 16), recorded for the first time in the gas phase, are markedly different from all other bands measured in the sense that in all other cases resolved rotational lines appear. The ν_3 and ν_4 excited state vibrational modes exhibit a triple-bond stretching vibration (cf. Fig. 17), which means that the molecule does not deviate from linearity. Hence, a rotational line separation is expected to be very similar to that of other $^2\Pi - ^2\Pi$ bands and rotational lines should be resolved in the same manner as for the other bands detected. Because this is not observed, it is assumed that the ν_3 and the ν_4 modes undergo lifetime broadening, most likely due to internal conversion. It is noted that the next carbon chain molecule in the $C_{2n}H$ series,

C_8H, also exhibits lifetime broadening already in its origin band.[38] For the moment, we leave the latter issues as outside the scope of the present work. Fluorescence studies, similarly as performed for the C_4H molecule,[39] might clarify some of the dynamics.

Since the stretching vibrations (which give rise to a state of total $^2\Pi$ symmetry) are all predicted upward from ~ 640 cm^{-1}, this leaves little space for assigning the other low frequency modes of total $^2\Pi$ symmetry. What remains to be considered are the following bands: Bands VII through XI and Bands XIII and XIV, while Band XVII is a special case, since its frequency is larger than the 650 cm^{-1} demarcation point between stretching and bending modes in C_6H.

Bands IX and X, detected for C_6H only, reproduce the characteristic structure of a $^2\Pi_\Omega$–$X^2\Pi_\Omega$ doublet. The derived value of $A' = -23.77$ cm^{-1} corresponds to the typical value for the spin-orbit constant also found for the 0_0^0 origin band and the ν_6 mode (Bands XV and XVI). In the neon matrix spectra[15] this band was observed at 19 286 cm^{-1}. The presently observed gas-phase $B^2\Pi_\Omega$–$X^2\Pi_\Omega$ doublet is thus shifted by 143 cm^{-1}, consistent with the typical gas-matrix shift for C_6H. This mode has an excitation energy of 439.5 cm^{-1}.

Bands XIII and XIV again display the typical characteristics of a $^2\Pi-{}^2\Pi$ doublet, but this assignment yields an excited state spin-orbit constant of $A' = -8.0$ cm^{-1}, which is atypical for the $B^2\Pi$ state. The vibrational mode has an excitation energy of 603 cm^{-1} above the band origin.

Band VIII, observed for both C_6H and $^{13}C_6H$, and Band XI observed only for C_6H, both display a characteristic of a $^2\Pi_{3/2} - {}^2\Pi_{3/2}$ component. In view of the fact that rotational fits could be made for the C_6H spectra, resulting in a rotational constant matching that of C_6H, the assignment of Bands VIII and XI to the C_6H molecule can be considered as unambiguous. Band VIII has, in C_6H, an excitation energy of 337 cm^{-1} above the origin, while in $^{13}C_6H$ it is at 324 cm^{-1}, consistent with the pattern of isotope shifts for the vibrational bands.

Band VII, observed for all three isotopologues, involves a $^2\Pi_{3/2} - {}^2\Pi_{3/2}$ component. The hypothesis that this component is overlaid with a $^2\Pi_{1/2} - {}^2\Pi_{1/2}$ component yields an upper state spin-orbit constant of $A' = -14.6$ cm^{-1}. This interpretation should however be considered as tentative. In any case, the assignment of the $^2\Pi_{3/2} - {}^2\Pi_{3/2}$ component may be considered as firm, as is the assignment of these bands to the C_6H molecule. Band VII lies at an excitation energy of 309 cm^{-1} for C_6H, and at 296 cm^{-1} for $^{13}C_6H$, again consistent with the isotopic pattern.

As for the vibrational levels of these bands, the modes with frequencies 308.8 cm^{-1}, 336.7 cm^{-1}, 439.5 cm^{-1}, and 603.3 cm^{-1}, hence below ~ 650 cm^{-1}, cannot be assigned to non-degenerate eigen modes. There simply are no stretching modes of such low energies predicted in the *ab initio* calculations[8–11] (see Table 2). Hence, the entire set of low-lying $^2\Pi$ states must be due to combination modes of bending vibrations, such as $2\nu_{11}$, $\nu_{11} + \nu_{10}$, $2\nu_{10}$, etc.

The observed spectrum of Band XVII is weak and only a band contour simulation has been possible. Its excitation energy of 937 cm^{-1} does not match with a stretching eigen mode in the *ab initio* calculations. The ν_5 stretching mode yields a consistent value close to $\sim 1\,210$ cm^{-1} in the *ab initio* calculations (cf. Table 2), which is off by ~ 300 cm^{-1} with respect to the band origin of Band XVII. If ν_5 is not covered by the band observed at 1 637.4 cm^{-1} (see above) then it might tentatively be assigned to the excitation at 937 cm^{-1}. Improved calculations of the $B^2\Pi$ excited electronic state vibrations of C_6H might decide on such a tentative assignment. Alternatively, and more probably, this feature could be due to a combination band, e.g., to a $2\nu_9$ mode. The observation that the B' rotational constants of several of these vibronic modes are larger than that of the 0_0^0 origin band implies that the vibration-rotation interaction is negative. This is typical for bending or bending-like modes, as was shown in the example of vibrations in the ground state of HC_6H.[40] This lends further credit to assigning the low-lying $^2\Pi$ states to bending combination modes.

The $^2\Sigma$ levels

In order to assign the remaining features in the recorded spectra interpreted as $^2\Sigma - {}^2\Sigma$ type bands, the interaction between degenerate electronic states and its fundamental bending modes, i.e., the Renner-Teller effect, has to be analyzed for a number of vibronically excited states of $^2\Sigma$ symmetry. In two sets of *ab initio* calculations performed for the electronic ground state,[9,10] some 5 doubly degenerate bending modes were calculated (using B3LYP hybrid functionals in Ref. [9]): ν_{11} at 110-120 cm^{-1}, ν_{10} at 214–255 cm^{-1}, ν_9 at 396–445 cm^{-1}, ν_8 at 519–553 cm^{-1}, and ν_7 at 561–679 cm^{-1}. Each of these give rise to a $\mu^2\Sigma - \kappa^2\Sigma$ doublet on the basis of which the five observed $^2\Sigma - {}^2\Sigma$ transitions are to be assigned.

The Hamiltonian describing the energy of vibronic states is given as the sum of the energies involved in pure vibration, in the RT coupling, and in the spin-orbit (SO) interaction:

$$H = H_{\rm vib} + H_{\rm RT} + H_{\rm SO}.$$

With the measured band origin T_0 for a particular transition, diagonalization of a matrix for calculated matrix elements for the various contributions will yield values of the true spin-orbit coupling constant ($A''_{\rm SO} = -47.5$ cm^{-1} and $A'_{\rm SO} = -23.74$ cm^{-1}) as well as for the Renner-Teller parameter ϵ, derived typically in the product $\epsilon\omega$,[17] with ω as the vibrational frequency. Then for $^2\Sigma$ vibronic states, the effective splitting A_Σ between

the two $^2\Sigma$ components (labeled as $\mu^2\Sigma$ and $\kappa^2\Sigma$) is given by:

$$A_\Sigma = \sqrt{{A_{SO}}^2 + 4\epsilon^2\omega^2} \quad (1)$$

and the effective rotational constants can be approximated as:[36,41]

$$B_{\text{eff}}^{\mu/\kappa} = B\left(1 \pm \frac{{A_{SO}}^2 B}{{A_\Sigma}^3}\right) \quad (2)$$

$$\gamma_{\text{eff}}^{\mu/\kappa} = 2B\left(1 - \frac{2\epsilon\omega}{A_\Sigma} \pm \frac{{A_{SO}}^2 B}{{A_\Sigma}^3}\right). \quad (3)$$

Such a RT analysis can be performed for the two low-lying bending modes ν_{10} and ν_{11}. For the lowest $\nu_{11} = 1$ vibrational mode, this was previously done for the C_6H and C_6D molecule, forming the basis for an assignment of a $\{11\}_1^1\ \mu^2\Sigma - \mu^2\Sigma$ transition.[17] A large RT parameter was obtained for the ground state ($\epsilon''_{11} \sim 0.99$), while a much smaller value was found for the excited state ($\epsilon'_{11} \sim 0.09$).

The presently observed Band III of $^{13}C_6H$ can be assigned in an analogous manner. On the basis of isotopic regularity, no other band feature is observed between this band and the (0,0) origin band of $^2\Pi - {}^2\Pi$ signature (combined Bands I and II). As listed in Table 1, the isotopic shifts of the first three observed bands of $^{13}C_6H$ are decreasing; Band III is consistent with this trend, having a band shift of 0.1 cm^{-1} to higher energy compared to the regular isotopologue C_6H. In addition, its band contour appears very similar as in the other isotopologues. Together with the results of the rotational line fit, all of these support for an unambiguous assignment of Band III in $^{13}C_6H$.

Furthermore, the RT analysis for the $\nu_{11} = 1$ mode in the upper electronic state predicts energy levels in the form of $^2\Sigma$ and $^2\Delta$ pairs, with the $\{11\}^1\ \kappa^2\Sigma$ level lying ~ 30 cm^{-1} above the $\{11\}^1\ \mu^2\Sigma$ level. No bands with nearly similar features have been observed in the predicted energy range, for neither of the three isotopologues. In general, a stronger RT effect in the upper state weakens the $\kappa^2\Sigma - \mu^2\Sigma$ transition which indicates a lesser coupling intensity between vibrational and electronic orbital angular momenta. In case of a strong Renner-Teller effect, the Π electronic orbital is coupled to a vibrational angular momentum (of Π symmetry), resulting into two Σ and one Δ vibronic states, where the two Σ states have different parity signs ($^2\Sigma^+$ and $^2\Sigma^-$). The transition to a pure $^2\Sigma^-$ state, from the $\mu^2\Sigma^+$ ground state becomes forbidden.[36,41] Apparently, the value of ϵ'_{11} is large enough to prohibit an observable intensity in the $\kappa^2\Sigma$ component, and indeed no band with a substantial S/N is found at the expected position for neither of the three isotopologues. Transitions to the $^2\Delta_{5/2}$ and $^2\Delta_{3/2}$ also cannot be observed since the only populated vibronic component of the ground $\nu_{11} = 1$ vibrational mode is the $\{11\}_1\ \mu^2\Sigma$ state and the selection rule does not allow for a change in vibronic symmetry greater than by one quantum number.

For the low-lying $\nu_{10} = 1$ bending mode in the $B^2\Pi$ excited state, a similar RT analysis can be performed yielding a μ-κ doublet of $^2\Sigma$ symmetry. Experimentally, from the characteristic shapes of Bands IV and V, one can infer that they start from the same ground state, and that they are excited to coupled vibronic levels. Indeed, from the rotational fit, both of these bands can be simulated using the same ground state constants which are those of the $\{11\}_1\ \mu^2\Sigma$ state. Moreover, the B' rotational constants for both bands are rather similar, as expected for a RT doublet.

The observed difference between the two band origins (~ 23 cm^{-1}) corresponds to the splitting A_Σ^{obs} between the $\mu^2\Sigma$ and the $\kappa^2\Sigma$ doublet. In contrast to the case of the ν_{11} bending mode, the combination of Bands IV and V may be interpreted as a doublet of transitions to the $\{10\}^1\ \mu^2\Sigma$ lower and $\{10\}^1\ \kappa^2\Sigma$ upper states of the RT doublet. If the value of the true spin-orbit constant $A'_{SO} = -23.74$ cm^{-1}, as determined from the analysis of ν_{11} is adopted, then an effective splitting between the band origins is calculated at $|A_\Sigma^{\text{calc}}| > |A_\Sigma^{\text{obs}}|$, via Eq. (1). This hints at the one side to a very small Renner-Teller parameter ($\epsilon'_{10} < 0.01$) but still, the splitting between band origins for $\{10\}^1\ \kappa^2\Sigma$ and $\{10\}^1\ \mu^2\Sigma$ is too small for a consistent analysis. It is likely that the $\{10\}^1\ \kappa^2\Sigma$ component (Band V) is shifted downwards, for example, due to a perturbation or a Fermi resonance. The fact that the γ' parameter for Band V, specifically for the C_6H isotopologue ($\gamma' = 0.107$ cm^{-1}), corresponds to $\gamma' > 2B'$ makes it unphysical and also points at a perturbation. In any case, the ϵ'_{10} value is expected to be small because both RT components are observed in the spectrum for all three isotopologues.

The next band observed, Band VI, also exhibits the character of a $^2\Sigma - {}^2\Sigma$ transition. Here, as in the case of the lowest ν_{11}, no second component in a μ-κ RT pair is observed. In view of the numbering of bending vibrations, Band VI may be assigned as the lower μ component of ν_9. In principle, the next band of $^2\Sigma - {}^2\Sigma$ character (Band XII) might be considered as the upper κ component of ν_9. However, the B' rotational constants for these bands differ substantially while they should be similar in a RT pair. For this reason, the last $^2\Sigma - {}^2\Sigma$ transition (Band XII) is tentatively assigned as the μ component of ν_8.

Isotope shifts

Table 1 displays values for the isotope shifts for the bands observed for $^{13}C_6H$ and C_6D with respect to those of C_6H. It should be noted that isotope shifts are determined only for degenerate bending modes, that is, for the $^2\Sigma - {}^2\Sigma$ vibronic bands or for combinations thereof.

The values can be understood by assuming that the effect of zero-point vibration makes up for a decisive contribution. If the ground state potential hypersurface is considered to be deeper than for the excited state, i.e., stronger chemical binding in the ground state, this explains the blue shift of the origin bands for the heavier molecules. The effect appears to be much stronger for C_6D than for $^{13}C_6H$ in view of the larger mass difference between D and H. For gradually higher vibrational excitation a regular effect of redshift for higher modes is observed of overall $\sim 10\ \mathrm{cm}^{-1}$ for eigen modes up to $\sim 300\ \mathrm{cm}^{-1}$. While for $^{13}C_6H$ the shift pattern develops smoothly and linearly, for C_6D the pattern is less regular. There is an outlier for Band V, which may be associated with the perturbation found in the Renner-Teller splitting of Bands IV and V. A perturbation-induced down shifting of Band V in C_6H will result in an increased isotope shift for C_6D and a decreased isotope shift for $^{13}C_6H$ (cf. Fig. 1). Indeed, the isotope shift of Band V for $^{13}C_6H$ deviates somewhat ($\sim 2\ \mathrm{cm}^{-1}$) from a smooth regular progression of isotope shifts.

The measured isotope shifts in the present study all pertain, except for the origin band, to degenerate vibrational modes or combinations thereof. It is found that isotopic shifts for these bands in $^{13}C_6H$ and C_6D behave very differently, while in C_6D the isotope shift is $\sim 50\ \mathrm{cm}^{-1}$, for $^{13}C_6H$ this is typically $\sim -5\ \mathrm{cm}^{-1}$, hence of opposite sign. Brown et al.[9] have performed specific isotope shift calculations for the non-degenerate ν_2 vibrational mode (reassigned from ν_3 in their paper) yielding a similar value of 78 cm^{-1} for both isotope shifts of $^{13}C_6H$ and C_6D (with respect to C_6H). This finding seems difficult to reconcile with the present measurements. Refined isotope shift calculations for a variety of bands may settle this issue.

Conclusion

The present study reports a comprehensive investigation of the vibronic structure of the $B^2\Pi$–$X^2\Pi$ transition in the C_6H molecule in the gas phase. Some 19 bands or band components have been detected, and in most cases rotationally resolved, for the main C_6H isotopologue, while eight have been recorded for $^{13}C_6H$ and seven for C_6D. All assignments, taking into account all the arguments given here, result in a rather complete energy level diagram for C_6H (Fig. 18) in which the observed transitions (with corresponding band labeling) are shown. This figure includes energies pertaining to the C_6H main isotopologue; corresponding values for $^{13}C_6H$ and C_6D can be obtained from Table 1. For the non-degenerate (Σ) vibrations, besides the 0_0^0 origin band three vibrational eigen modes have been identified: ν_6, ν_3, and, tentatively, ν_4. In addition, a number of excited $^2\Pi$ vibronic states have been assigned to be probed in combination bands involving two low-lying degenerate vibrations. Low-lying bending modes have been observed for which a Renner-Teller treatment has been applied unambiguously, leading to the assignment of the $\mu^2\Sigma$ component of the ν_{11} mode and both $\mu^2\Sigma$ and $\kappa^2\Sigma$ components of the ν_{10} mode, while the $\mu^2\Sigma$ components of ν_9 and ν_8 have been tentatively assigned. These assignments are based on *ab initio* calculations of the C_6H molecule, which were however carried out for the ground state electronic configuration of the molecule.[8–10] Previous matrix isolation data[14,15] and higher temperature discharge spectra[16] were useful in the analysis, as were the present results on the $^{13}C_6H$ and C_6D isotopologues. The analysis and descriptive detail of the level structure of C_6H now equals that of the C_4H molecule[39] which is part of the same C_nH carbon chain series.

The present comprehensive experimental study might be a stimulus for future *ab initio* calculations specifically focusing on the $B^2\Pi$ electronically excited state of C_6H. Some open issues remain; those are the quest for a definite assignment of some vibrational (combination) modes, perturbation effects, and the dynamical effect of internal conversion in the highest vibrational levels. The investigation of the optical spectra of carbon chain molecules, and in particular also the C_6H molecule, was originally driven by the hypothesis that $^2\Pi - {}^2\Pi$ electronic transitions of C_nH radicals might be responsible for some of the diffuse interstellar bands[42] observed in the optical spectra of reddened stars. For the presently observed manifold of vibronic bands this is not the case.

Acknowledgements

This work has been supported by the Netherlands Organization for Scientific Research (NWO) through a VICI grant and was performed within the context of the Dutch Astrochemistry Network (DAN).

References

[1] Suzuki, H.; Ohishi, M.; Kaifu, N.; Ishikawa, S. I.; Kasuga, T. *Publ. Astron. Soc. Jpn.* **1986**, *38*, 911–917.
[2] Cernicharo, J.; Guélin, M.; Menten, K. M.; Walmsley, C. M. *Astron. Astrophys.* **1987**, *181*, L1–L4.
[3] Guélin, M.; Cernicharo, J.; Gomez-Gonzalez, J.; Walmsley, C. M. *Astron. Astrophys.* **1987**, *175*, L5–L8.
[4] Kawaguchi, K.; Kasai, Y.; Ishikawa, S.-I.; Kaifu, N. *Publ. Astron. Soc. Jpn.* **1995**, *47*, 853–876.
[5] Pearson, J. C.; Gottlieb, C. A.; Woodward, D. R.; Thaddeus, P. *Astron. Astrophys.* **1988**, *189*, L13–L15.
[6] Linnartz, H.; Motylewski, T.; Vaizert, O.; Maier, J. P.; Apponi, A. J.; McCarthy, M. C.; Gottlieb, C. A.; Thaddeus, P. *J. Mol. Spectrosc.* **1999**, *197*, 1–11.
[7] Gottlieb, C. A.; McCarthy, M. C.; Thaddeus, P. *Astrophys. J. Suppl. S.* **2010**, *189*, 261–269.

[8] Liu, R.; Zhou, X.; Pulay, P. *J. Chem. Phys.* **1992**, *97*, 1602–1605.
[9] Brown, S. T.; Rienstra-Kiracofe, J. C.; Schaefer III, H. F. *J. Phys. Chem. A* **1999**, *103*, 4065–4077.
[10] Cao, Z.; Peyerimhoff, S. D. *Phys. Chem. Chem. Phys.* **2001**, *3*, 1403–1406.
[11] Doyle, T.; Shen, L.; Rittby, C.; Graham, W. *J. Chem. Phys.* **1991**, *95*, 6224–6228.
[12] Cernicharo, J.; Guélin, M.; Agúndez, M.; McCarthy, M. C.; Thaddeus, P. *Astrophys. J.* **2008**, *688*, L83–L86.
[13] McCarthy, M.; Gottlieb, C.; Gupta, H.; Thaddeus, P. *Astrophys. J. Lett.* **2006**, *652*, L141.
[14] Forney, D.; Fulara, J.; Freivogel, P.; Jakobi, M.; Lessen, D.; Maier, J. P. *J. Chem. Phys.* **1995**, *103*, 48–53.
[15] Freivogel, P.; Fulara, J.; Jakobi, M.; Forney, D.; Maier, J. P. *J. Chem. Phys.* **1995**, *103*, 54–59.
[16] Kotterer, M.; Maier, J. P. *Chem. Phys. Lett.* **1997**, *266*, 342–346.
[17] Zhao, D.; Haddad, M. A.; Linnartz, H.; Ubachs, W. *J. Chem. Phys.* **2011**, *135*, 044307.
[18] Taylor, T. R.; Xu, C.; Neumark, D. M. *J. Chem. Phys.* **1998**, *108*, 10018–10026.
[19] Sobolewski, A. L.; Adamowicz, L. *J. Chem. Phys.* **1995**, *102*, 394–399.
[20] Shnitko, I.; Fulara, J.; Batalov, A.; Gillery, C.; Masso, H.; Rosmus, P.; Maier, J. P. *J. Phys. Chem. A* **2006**, *110*, 2885–2889.
[21] Raghunandan, R.; Mazzotti, F. J.; Maier, J. P. *J. Am. Soc. Mass Spectr.* **2010**, *21*, 694–697.
[22] Motylewski, T.; Linnartz, H. *Rev. Sci. Instrum.* **1999**, *70*, 1305–1312.
[23] Zhao, D.; Wehres, N.; Linnartz, H.; Ubachs, W. *Chem. Phys. Lett.* **2011**, *501*, 232–237.
[24] Wheeler, M. D.; Newman, S. M.; Orr-Ewing, A. J.; Ashfold, M. N. *J. Chem. Soc., Faraday Trans.* **1998**, *94*, 337–351.
[25] Haddad, M.; Zhao, D.; Linnartz, H.; Ubachs, W. *Mol. Phys.* **2015**, *113*, 2063–2072.
[26] Zhao, D.; Haddad, M. A.; Linnartz, H.; Ubachs, W. *J. Chem. Phys.* **2011**, *135*, 074201.
[27] Zhao, D.; Linnartz, H.; Ubachs, W. *J. Chem. Phys.* **2012**, *136*, 054307.
[28] Lloyd, G. M.; Ewart, P. *J. Chem. Phys.* **1999**, *110*, 385–392.
[29] PGOPHER, a Program for Simulating Rotational Structure, C. M. Western, University of Bristol, http://pgopher.chm.bris.ac.uk.
[30] Nagarajan, R.; Maier, J. P. *Int. Rev. Phys. Chem.* **2010**, *29*, 521–554.
[31] Bacalla, X.; Zhao, D.; Salumbides, E. J.; Haddad, M. A.; Linnartz, H.; Ubachs, W. *J. Mol. Spectrosc.* **2015**, *308-309*, 41–44.
[32] Herzberg, G. *Molecular Spectra and Molecular Structure I. Spectra of Diatomic Molecules,*; D. Van Nostrand: New York, 1950.
[33] Pfluger, D.; Motylewski, T.; Linnartz, H.; Sinclair, W. E.; Maier, J. P. *Chem. Phys. Lett.* **2000**, *329*, 29–35.
[34] Denisov, A. Electronic Spectroscopy of Unsaturated Hydrocarbons and Sulfur-Terminated Carbon Chains by Cavity Ringdown. Ph.D. thesis, Universität Basel, 2006.
[35] Araki, M.; Cias, P.; Denisov, A.; Fulara, J.; Maier, J. P. *Can. J. Chem.* **2004**, *82*, 848–853.
[36] Herzberg, G. *Molecular Spectra and Molecular Structure III. Electronic Spectra and Electronic Structure of Polyatomic Molecules*; D. Van Nostrand: New York, 1966; pp 181–183.
[37] Pauzat, F.; Ellinger, Y. *Astron. Astrophys.* **1989**, *216*, 305–309.
[38] Birza, P.; Khoroshev, D.; Chirokolava, A.; Motylewski, T.; Maier, J. P. *Chem. Phys. lett.* **2003**, *382*, 245–248.
[39] Hoshina, K.; Kohguchi, H.; Ohshima, Y.; Endo, Y. *J. Chem. Phys.* **1998**, *108*, 3465–3478.
[40] Chang, C.-H.; Agarwal, J.; Allen, W. D.; Nesbitt, D. J. *J. Chem. Phys.* **2016**, *144*, 074301.
[41] Hougen, J. T. *J. Chem. Phys.* **1962**, *36*, 519–534.
[42] Fulara, J.; Lessen, D.; Freivogel, P.; Maier, J. *Nature* **1993**, *366*, 439–441.

Table 1: Summary of spectroscopic constants in cm^{-1}. Terminating the values (enclosed in parentheses) are the statistical uncertainties (1σ) obtained from a least-squares rotational line fit. For values obtained through a band contour simulation, the uncertainties are omitted. Numbers in italics are electronic ground state values taken from Refs. [6] and [7] and are kept fixed in the fitting routine (with the exception for $^{13}C_6H$). Tentative mode assignments are enclosed in square brackets [ ].

		T_0 [a]	Band type	B'	B''	γ' (10^{-3})	γ'' (10^{-3})	A'	A''	Relative energy	Isotopic shift [b]	Assignment [c]
C_6H	I, II[d]	18989.7672(4)	$^2\Pi - ^2\Pi$	0.0455952(5)	*0.04640497*	−3.63(18)	*−7.12*	−23.69(2)	*−15.04*	0.0	-	0_0^0
	III[d]	19066.8372(6)	$^2\Sigma - ^2\Sigma$	0.0456873(11)	*0.04652018*	38.29(6)	*−0.628*	-	-	77.1	-	$\mu\{11\}_1^1$ bend
	IV	19197.314(3)	$^2\Sigma - ^2\Sigma$	0.045580(7)	*0.04652018*	79.55(18)	*−0.628*	-	-	207.5	-	$\mu\{10\}^1\,\mu\{11\}_1$ bend
	V	19220.294(6)	$^2\Sigma - ^2\Sigma$	0.045971(18)	*0.04652018*	107.1(4)	*−0.628*	-	-	230.5	-	$\kappa\{10\}^1\,\mu\{11\}_1$ bend
	VI	19283.992(3)	$^2\Sigma - ^2\Sigma$	0.045916(8)	*0.04652018*	70.27(16)	*−0.628*	-	-	294.2	-	[$\mu\{9\}^1\,\mu\{11\}_1$] bend
	VII	19298.56[e]	$^2\Pi - ^2\Pi$	0.0457[e]	*0.04640497*	40[e]	*−7.12*	−14.6[ef]	*−15.04*	308.8	-	
	VIII	19326.479(4)	$^2\Pi - ^2\Pi$	0.045392(11)	*0.04640497*	-	-	-	-	336.7	-	
	IX, X	19429.236(5)	$^2\Pi - ^2\Pi$	0.046137(12)	*0.04640497*	−7(6)	*−7.12*	−23.77(2)	*−15.04*	439.5	-	
	XI	19451.792(2)	$^2\Pi - ^2\Pi$	0.045969(5)	*0.04640497*	-	-	-	-	462.0	-	
	XII	19486.08[e]	$^2\Sigma - ^2\Sigma$	0.0455[e]	*0.04652018*	13[e]	*−0.628*	-	-	496.3	-	[$\mu\{8\}^1\,\mu\{11\}_1$] bend
	XIII, XIV	19593.11[e]	$^2\Pi - ^2\Pi$	0.0456[e]	*0.04640497*	-	-	−8.0[e]	*−15.04*	603.3	-	
	XV, XVI	19648.7[e]	$^2\Pi - ^2\Pi$	0.0460[e]	*0.04640497*	-	-	−24.4[e]	*−15.04*	658.9	-	$\{6\}_0^1$ stretch
	XVII	19926.41[e]	$^2\Pi - ^2\Pi$	0.0460[e]	*0.04640497*	-	-	−14.50[ef]	*−15.04*	936.6	-	
	XVIII	20627.2[e]	$^2\Pi - ^2\Pi$	0.0461[e]	*0.04640497*	−40[e]	*−7.12*	−20.3[e]	*−15.04*	1637.4	-	[$\{4\}_0^1$] stretch
	XIX	21070.6[e]	$^2\Pi - ^2\Pi$	0.0454[e]	*0.04640497*	30[e]	*−7.12*	−16.8[e]	*−15.04*	2080.8	-	$\{3\}_0^1$ stretch
$^{13}C_6H$	I, II[g]	18992.116(1)	$^2\Pi - ^2\Pi$	0.042218(17)	0.042973(16)	-	-	−20.78(13)	−11.62(13)	0.0	2.3	0_0^0
	III	19066.9716(16)	$^2\Sigma - ^2\Sigma$	0.04227(4)	0.04308(4)	34(3)	−4(3)	-	-	74.9	0.1	$\mu\{11\}_1^1$ bend
	IV	19192.1414(17)	$^2\Sigma - ^2\Sigma$	0.042235(3)	*0.04308*	69.72(11)	*−4*	-	-	200.0	−5.2	$\mu\{10\}^1\,\mu\{11\}_1$ bend
	V	19215.202(2)	$^2\Sigma - ^2\Sigma$	0.042443(5)	*0.04308*	90.22(15)	*−4*	-	-	223.1	−5.1	$\kappa\{10\}^1\,\mu\{11\}_1$ bend
	VI	19274.22[e]	$^2\Sigma - ^2\Sigma$	0.0422[e]	*0.04308*	−4[e]	*−4*	-	-	282.1	−9.8	[$\mu\{9\}^1\,\mu\{11\}_1$] bend
	VII	19288.62[e]	$^2\Pi - ^2\Pi$	0.0423[e]	*0.04297*	-	-	−11.40[ef]	*−11.62*	296.5	−9.9	
	VIII	19316.45[e]	$^2\Pi - ^2\Pi$	0.0425[e]	*0.04297*	-	-	-	-	324.3	−10.0	
C_6D	I, II[d]	19041.2564(5)	$^2\Pi - ^2\Pi$	0.043592(4)	*0.04429243*	−6.3(7)	*−3.85*	−24.07(2)	*−15.13*	0.0	51.5	0_0^0
	III[d]	19115.5251(10)	$^2\Sigma - ^2\Sigma$	0.0436478(19)	*0.0443852*	39.68(10)	*−0.631*	-	-	74.3	48.7	$\mu\{11\}_1^1$ bend
	IV	19243.221(2)	$^2\Sigma - ^2\Sigma$	0.043638(5)	*0.0443852*	57.89(11)	*−0.631*	-	-	202.0	45.9	$\mu\{10\}^1\,\mu\{11\}_1$ bend
	V	19271.454(5)	$^2\Sigma - ^2\Sigma$	0.043721(11)	*0.0443852*	64.6(3)	*−0.631*	-	-	230.2	51.2	$\kappa\{10\}^1\,\mu\{11\}_1$ bend
	VI	19327.10[e]	$^2\Sigma - ^2\Sigma$	0.0429[e]	*0.0443852*	−1[e]	*−0.631*	-	-	285.8	43.1	[$\mu\{9\}^1\,\mu\{11\}_1$] bend
	VII	19342.16[e]	$^2\Pi - ^2\Pi$	0.0435[e]	*0.04429243*	-	-	−14.68[ef]	*−15.13*	300.9	43.6	

Note: Except for Bands I and II and for Band III, we assume $D' \approx D''$: 1.35×10^{-9} cm^{-1} (C_6H) and 1.2×10^{-9} cm^{-1} ($^{13}C_6H$ and C_6D).

[a] Resulting values from the fitting routine, but the absolute uncertainty is limited to 0.02 cm^{-1} from I_2 calibration.
[b] Relative to the corresponding band in C_6H.
[c] The notation, e.g. $\kappa\{10\}^1\,\mu\{11\}_1$, denotes a transition from the μ component of the $\nu_{11} = 1$ vibrational mode of the lower electronic state to the κ component of the $\nu_{10} = 1$ mode of the upper electronic state. The mode numbering is adopted from Ref. [9].
[d] Data from Ref. [17].
[e] Value obtained from band contour simulation.
[f] Tentative value, derived from the assumption that the $^2\Pi_{1/2}$ component overlaps the $^2\Pi_{3/2}$ component.
[g] Data from Ref. [31].

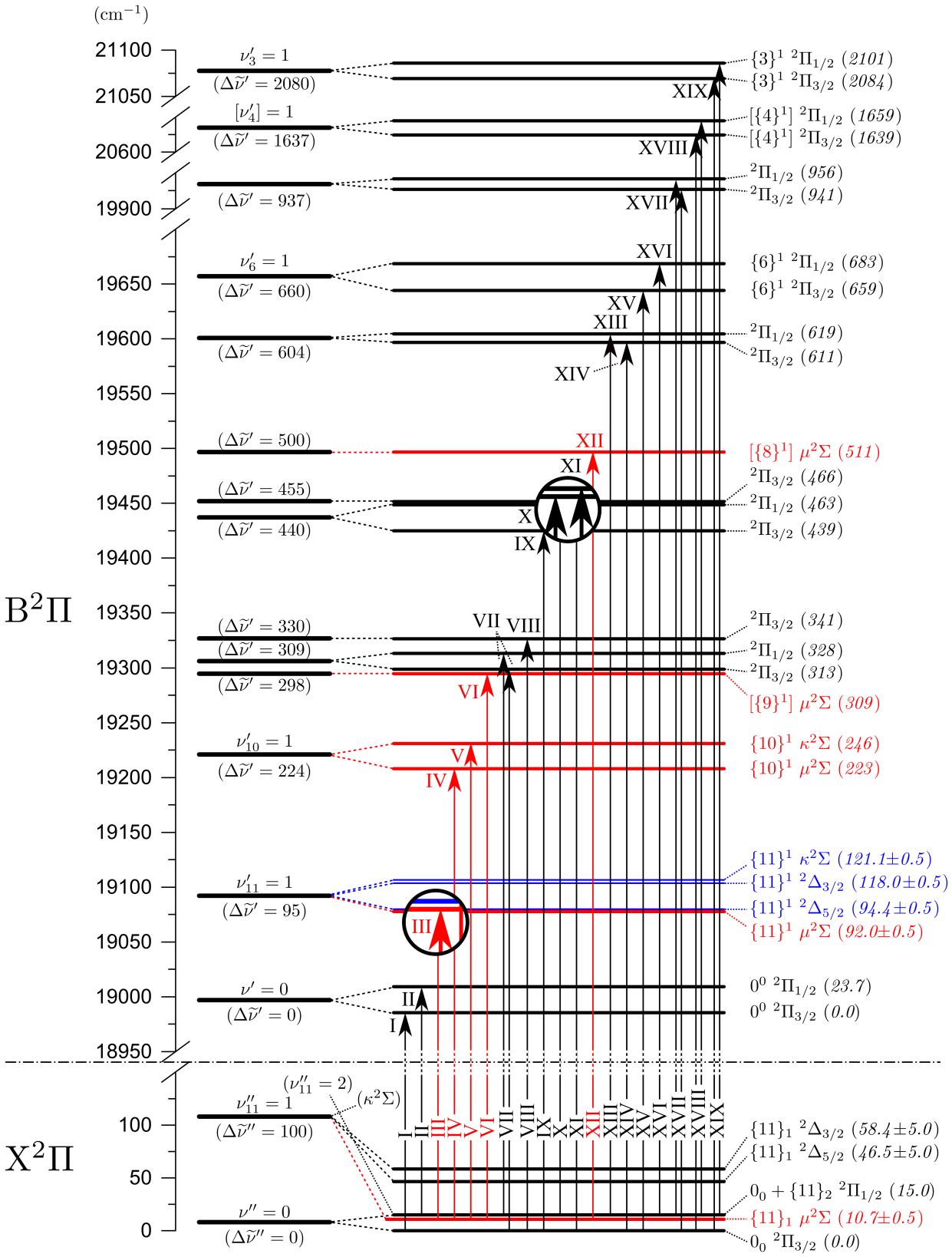

Figure 18: Energy level diagram for C_6H. The line cutting across the diagram separates the ground $X^2\Pi$ electronic state from the excited $B^2\Pi$ state. As plasma jets produce vibrationally cold molecules, all observed transitions originate from the lowest lying states: $0_0\ ^2\Pi_{3/2}$, $0_0\ ^2\Pi_{1/2}$, and $\{11\}_1\ \mu^2\Sigma$, with the $^2\Sigma - {}^2\Sigma$ transitions in red. Numbers in parentheses () are the vibrational (left) and vibronic (right) frequencies expressed relative to the respective vibrational and vibronic ground states for each of the electronic states. States that are thus far unobserved experimentally are indicated in blue. Tentative mode identifications are given in square brackets [ ]. Vibrational eigen modes are according to the numbering in Brown et al. [9].